Author Manuscript

Author Manuscript

Author Manuscript

Author Manuscript

HHS Public Access

Author manuscript

J Mol Cell Cardiol. Author manuscript; available in PMC 2022 March 01.

Published in final edited form as:

J Mol Cell Cardiol. 2021 March ; 152: 1–16. doi:10.1016/j.yjmcc.2020.11.009.

Protective role of ErbB3 signaling in myeloid cells during adaptation to cardiac pressure overload

Haifeng Yin[1], **Amanda J. Favreau-Lessard**[1], **Joanne T. deKay**[1], **Yodit R Herrmann**[1], **Michael P. Robich**[1,2], **Robert A. Koza**[1], **Igor Prudovsky**[1], **Douglas B. Sawyer**[1,2], **Sergey Ryzhov**[1]

[1]Maine Medical Center Research Institute, Scarborough, ME

[2]Maine Medical Center, Cardiovascular Institute, Portland, ME

Abstract

Background—Myeloid cells play an important role in a wide variety of cardiovascular disorders, including both ischemic and non-ischemic cardiomyopathies. Neuregulin-1 (NRG-1)/ErbB signaling has recently emerged as an important factor contributing to the control of inflammatory activation of myeloid cells after an ischemic injury. However, the role of ErbB signaling in myeloid cells in non-ischemic cardiomyopathy is not fully understood. This study investigated the role of ErbB3 receptors in the regulation of early adaptive response using a mouse model of transverse aortic constriction (TAC) for non-ischemic cardiomyopathy.

Methods and results—TAC surgery was performed in groups of age- and sex-matched myeloid cell-specific ErbB3-deficient mice ($ErbB3^{MyeKO}$) and control animals ($ErbB3^{MyeWT}$). The number of cardiac CD45 immune cells, CD11b myeloid cells, Ly6G neutrophils, and Ly6C monocytes was determined using flow cytometric analysis. Five days after TAC, survival was dramatically reduced in male but not female $ErbB3^{MyeKO}$ mice or control animals. The examination of lung weight to body weight ratio suggested that acute pulmonary edema was present in $ErbB3^{MyeKO}$ male mice after TAC. To determine the cellular and molecular mechanisms involved in the increased mortality in $ErbB3^{MyeKO}$ male mice, cardiac cell populations were examined at day 3 post-TAC using flow cytometry. Myeloid cells accumulated in control but not in $ErbB3^{MyeKO}$ male mouse hearts. This was accompanied by increased proliferation of Sca-1 positive non-immune cells (endothelial cells and fibroblasts) in control but not $ErbB3^{MyeKO}$ male mice. No significant differences in intramyocardial accumulation of myeloid cells or proliferation of Sca-1 cells were found between the groups of $ErbB3^{MyeKO}$ and $ErbB3^{MyeWT}$ female mice. An antibody-based protein array analysis revealed that IGF-1 expression was significantly downregulated only in $ErbB3^{MyeKO}$ mice hearts compared to control animals after TAC.

*Address for correspondence and reprint requests: Sergey Ryzhov, PhD, Maine Medical Center Research Institute, 81 Research Drive, Scarborough, ME 04074, 207-396-8279 (phone); 207-396-8179 (fax); sryzhov@mmc.org.

DISCLOSURES

None

Publisher's Disclaimer: This is a PDF file of an unedited manuscript that has been accepted for publication. As a service to our customers we are providing this early version of the manuscript. The manuscript will undergo copyediting, typesetting, and review of the resulting proof before it is published in its final form. Please note that during the production process errors may be discovered which could affect the content, and all legal disclaimers that apply to the journal pertain.

Author Manuscript Author Manuscript Author Manuscript Author Manuscript

Conclusion: Our data demonstrate the crucial role of myeloid cell-specific ErbB3 signaling in the cardiac accumulation of myeloid cells, which contributes to the activation of cardiac endothelial cells and fibroblasts and development of an early adaptive response to cardiac pressure overload in male mice.

Keywords

transverse aortic constriction; non-ischemic cardiomyopathy; ErbB3; myeloid cells; insulin growth factor-1

1. INTRODUCTION

Immune cells play various and diverse roles during the initiation and progression of cardiomyopathy, as well as in the transition of cardiomyopathy to heart failure, a major cause of morbidity and mortality[1]. The role of the immune response in ischemic cardiomyopathy and heart failure has been intensively investigated during the last two decades [2-6]. In contrast, the role of the immune cells in the pathophysiology of non-ischemic cardiomyopathy is less clear [7]. Studies in patients with idiopathic dilated cardiomyopathy demonstrated activation of neutrophils[8, 9], and a shift in subpopulations of lymphocytes toward lower T-suppressor frequencies[10], indicating the potential involvement of the immune system in non-ischemic cardiomyopathy.

In animal studies, transverse aortic banding[11] is widely used to investigate the mechanisms of immune cell contribution to non-ischemic injury. In this model, the increased cardiac afterload induces the development of adaptive left ventricular hypertrophy, followed by maladaptive heart failure[12]. Immune cells infiltrate pressure overload-stressed myocardium as early as day three after the surgery, with blood neutrophils and monocytes being the first immune cell types entering the heart[13, 14]. Within the first week after pressure overload, cardiac macrophages undergo proliferation and increase in numbers[15, 16]. While the relationships between different subsets of myeloid cells require further investigation, recent studies indicate that neutrophils, monocytes, and macrophages play a role in the modulation of early adaptive responses and development of hypertrophy[14, 17]. In contrast to myeloid cells, lymphocytes accumulate in the myocardium later and contribute to the transition from hypertrophy to heart failure[18, 19].

The ErbB family of receptor tyrosine kinases regulates cardiac inflammation. This family consists of four members: ErbB1, also known as epidermal growth factor receptor, ErbB2, ErbB3, and ErbB4[20]. ErbB receptor ligands are peptides, the majority of which are generated by proteolytic cleavage of membrane-bound growth factors such as epidermal growth factor or neuregulins[21, 22]. Clinical trials have demonstrated the beneficial therapeutic effects of neuregulin-1 on left ventricular function in patients with heart failure [23]. However, the effect of neuregulin-1 on the immune system has not been evaluated in those studies. Limited data indicate that ErbB1 is expressed on monocytes and regulates their function[24, 25]. However, it is unclear whether the ErbB1/monocyte axis plays a role in cardiac inflammation. ErbB2 receptors have no ligand-binding activity and are reliant on heterodimerization with ErbB1, ErbB3, or ErbB4.

Author Manuscript Author Manuscript Author Manuscript Author Manuscript

Several studies have demonstrated that ErbB3 and ErbB4 are involved in the control of inflammation in the cardiovascular system, mostly via signaling in myeloid cells. The expression of ErbB4 is significantly upregulated during activation of monocytes and macrophages, and ligand-dependent stimulation of ErbB4 results in the induction of apoptosis in inflammatory macrophages[26]. The depletion of ErbB4 expression in myeloid cells in mice is associated with increased myocardial inflammation induced by angiotensin II[27].

We have recently demonstrated that neuregulin-1-dependent activation of ErbB3 reduces proinflammatory activation of nonclassical monocytes obtained from patients with heart failure[28]. However, the role of ErbB3 in local myocardial inflammation has not been studied. Here, we investigated the role of myeloid ErbB3 signaling using a mouse model of transverse aortic constriction. We demonstrate an early mortality effect on male mice with ErbB3 deletion in myeloid cells. Our data reveal the novel roles of ErbB3 signaling in the regulation of myocardial accumulation of immune cells, proliferation of Sca-1 mesenchymal cells, and production of IGF-1 in response to cardiac pressure overload.

2. METHODS

All data that support the findings of this study are available from the corresponding author upon reasonable request.

2.1. Animals

All experiments were conducted in accordance with the Guide for the Care and Use of Laboratory Animals as adopted and promulgated by the US National Institutes of Health. Animal studies were reviewed and approved by the Institutional Animal Care and Use Committee of Maine Medical Center Research Institute. ErbB3$^{fl/fl}$ mice (FVB background) were a generous gift from Dr. Rebecca Cook, Vanderbilt University. LysM-Cre mice (B6.129P2-Lyz2tm1(cre)Ifo/J) and FVB/NJ mice we obtained from Jackson Laboratory (Bar Harbor, ME). All of the LysM-Cre mice used in these studies were backcrossed to the FVB genetic background for more than ten generations. ErbB3^{MyeKO} mice, with ErbB3 deletion in myeloid cells, were generated by crossing ErbB3$^{fl/fl}$ and LysM-cre mice. ErbB3^{wt}/LysM-Cre+ (ErbB3^{MyeWT}) mice were used as control animals. Genotypes were confirmed by analyzing genomic DNA with primers in a polymerase chain reaction as described [29, 30]. Adult male and female mice were housed in groups of four on a 12-hour light-dark cycle. Mice were kept in a temperature and humidity-controlled room with free access to a regular low-fat chow diet and water. Male and female (50/50) mice at 16-20 weeks old were used in all experiments.

2.2. Reagents

Recombinant NRG-1 (extracellular domain, 377-HB) was purchased from Bio-Techne/R&D Systems. Collagenase II (345 units per mg, CLS-2) was purchased from Worthington Biochemical Corporation (Lakewood, NJ), dispase II (04942078001) was from Roche Life Science (Indianapolis, IN), and DNase I was from Sigma (St. Louis, MO). Recombinant

Author Manuscript Author Manuscript Author Manuscript Author Manuscript

mouse granulocyte-macrophage colony-stimulating factor (GM-CSF) and macrophage colony-stimulating factor (M-CSF) were obtained from BioLegend (San Diego, CA).

2.3. Transverse aortic constriction (TAC)

TAC surgery was performed as previously described [11, 31]. In brief, anesthetized mice placed on an isothermal pad were maintained on artificial ventilation. The transverse aorta was visualized through a sternotomy and 7-0 silk ligature was tied around the aorta between the right brachiocephalic and left common carotid arteries to generate 27-gauge constriction. The chest was closed in layers, and the animals were gradually weaned from the respirator. Sham-operated animals underwent the same surgical procedures except for TAC. The blood pressure gradient across the ligation site was confirmed by Doppler ultrasound imaging. Echocardiography was performed in conscious mice with a VisualSonics Vevo 2100 imaging system, as described previously [32]. LV function was recorded at parasternal short axis view in M-mode and calculated as a fractional shortening (FS).

2.4. Blood collection and preparation of spleen, cardiac and bone marrow cell suspension

Submandibular blood collection was performed using 5 mm GoldenRod Animal Lancets (Medipoint Inc, Mineola, NY, USA). Blood was collected into Eppendorf tubes containing a citrate-dextrose solution (ACD, Sigma). Erythrocytes were lysed using an ammonia chloride solution containing 1.5 M NH_4CL, 100 mM sodium bicarbonate, and 10 mM EDTA.

To prepare cell suspension, the spleen was excised and cut into small pieces and pressed through 70 μm strainer using a plunger end of the syringe. Cells were washed with Dulbecco's PBS and resuspended in PBS/0.5%BSA/2 mM EDTA after erythrocytes lysis.

Isolation of cardiac stromal cell populations was performed according to a protocol published previously [33]. In brief, minced tissue was incubated in digestion solution (10 mg/ml collagenase II, 2.5 U/ml dispase II, 1 μg/ml DNase I, and 2.5 mM $CaCl_2$) for 25 min at 37°C. After passing through a 70-μm cell strainer, the resulting myocyte-free single-cell suspension was centrifuged at 500 x *g*, washed with Dulbecco's PBS, and resuspended in PBS/0.5%BSA/2 mM EDTA.

Bone marrow cells were harvested from the femurs and tibias of $ErbB3^{MyeWT}$ or $ErbB3^{MyeKO}$ mice. Erythrocytes were lysed, cells were washed twice with PBS and used for isolation of lineage-negative (Lin-) hematopoietic progenitor cells, CD11b cells, differentiation and migration assay, and flow cytometric analysis.

2.5. Nuclear Magnetic Resonance (NMR) analysis

NMR analysis was performed as previously described[34]. In brief, mice were scanned using a Minispec NMR (Bruker Optics, Inc), which allows for non-invasive and rapid measurements of body composition without the use of anesthesia. Mice were placed in a plastic cylinder and kept immobile by insertion of a plunger into the cylinder. The plastic cylinder with the animal was placed in the sample chamber for the duration of the scan (approximately two minutes). The MiniSpec NMR uses contrasting hydrogen density/hydrogen spin properties

Author Manuscript Author Manuscript Author Manuscript Author Manuscript

from adipose tissue and lean mass for estimation of body composition. A quality control check of NMR parameters using a standard provided by the manufacturer was performed prior to each day of testing.

2.6. Heart tissue processing, histopathology and immunochistochemistry

Hearts were arrested with potassium and perfused with phosphate buffer saline. Excised hearts were immersion fixed in 10% buffered formalin for 24 hours and transferred to 70% ethanol. From each paraffin-embedded ventricular part, two transverse sections were made at different levels (for a total of six sections). Five-μm sections were prepared from paraffin blocks and stained with Hematoxylin and Eosin (H&E). Myocardial fibrosis was assessed after Masson's trichrome staining, and the fibrotic area was calculated as a percentage of total tissue area.

Rabbit monoclonal antibody against cleaved caspase 3 (D175, Cell Signaling Technology) at the dilution 1:250 was used to detect active apoptosis. The image analysis was performed by using an Axioskop 40 microscope equipped with a digital camera. All measurements were conducted using ImageJ software version 1.45s (NIH) in a blinded manner.

2.7. Flow cytometric analysis

Cells (10^6 cells/ml) were incubated with murine TruStain FcX™ reagent (BioLegend, San Diego, CA) to block non-specific binding, following by the incubation with relevant antibodies for 20-30 min at 4°C. Then cells were washed once with ten volumes of cold PBS/0.5% BSA/2 mM EDTA and used for the flow cytometric analysis.

Cell-surface antigen expression was examined using the following antibodies: anti-mouse CD11b (M1/70), CD31 (390), CD45 (30-F11), Ly6C (HK1.4), Ly6G (1A8), and Sca-1 (E13-161.7) (all purchased from BioLegend).

Phycoerythrin (PE)-conjugated rabbit polyclonal anti-EGFR (D38B1, Cell Signaling Technology) and rat monoclonal anti-ErbB2 (FAB6744P, Bio-techne/R&D System) were used for the analysis of cell surface expression of ErbB1 and ErbB2, respectively. Sheep anti-mouse ErbB3 (AF4518) and rabbit monoclonal anti-ErbB4 (111B2, Cell Signaling Technology) were conjugated with PE, using Mix-n-Stain™ R-PE Antibody Labeling Kit (Biotium, Fremont, CA) and used for detection of ErbB3 and ErbB4 at the cell surface of myeloid cells. To improve the detection of ErbB receptors, after initial staining with primary antibodies conjugated to PE, cells were stained with biotin anti-PE antibody (PE001, BioLegend) followed by additional staining with Streptavidin-PE (SAv-PE, BioLegend). This resulted in the two-fold increase in the fluorescence intensity corresponding to ErbB receptors without increasing background fluorescence.

Alexa Fluor 488-conjugated anti-phosphatidylserine antibody (1H6, Millipore/Sigma) was used to detect apoptotic cells.

Intracellular staining for IGF-1 was performed with PE-conjugated anti-IGF-1 antibody (NBP2-34679PE, Bio-Techne/Novus) in fixed and permeabilized cells using BD Cytofix/Cytoperm™ (BD Biosciences). Staining for proliferating cells with Ki-67 (16A8) was done

Author Manuscript Author Manuscript Author Manuscript Author Manuscript

using True-Nuclear™ Transcription Factor Buffer Set (BioLegend). All antibodies were titrated to establish a high separation between positive and negative cell populations while maintaining a low level of background. Isotype-matched control antibodies were used to determine the level of undesired non-specific binding. The expression of cell markers and ErbB receptors was determined after subtraction of the mean fluorescence intensity (MFI) of isotype-matched controls from the MFI of specific antibodies and represented as a delta mean fluorescence intensity (ΔMFI) as described elsewhere [35]. Antigen negativity was defined as having the same fluorescent intensity as the isotype control.

Data acquisition was performed on a MacsQuant Analyzer 10 (Miltenyi Biotec., Inc.), and the data were analyzed using WinList 5.0 software. Viable and non-viable cells were distinguished using DAPI (to detect dead nucleated cells) and LIVE/DEAD® Fixable Violet Stain kit for the detection of non-nucleated cell debris (Life Technologies, Carlsbad, CA).

2.8. Isolation of hematopoietic progenitor cells and CD11b myeloid cells

Untouched Lin- hematopoietic progenitor cells were purified from bone marrow cell suspension using the Lineage Cell Depletion Kit (Miltenyi Biotec, Inc). Isolated cells were incubated in the presence of 20 ng/ml of GM-CSF or 20 ng/ml of M-CSF for six days (with medium renewal at day three) to generate mature myeloid cells, which corresponds to a more proinflammatory phenotype (GM-CSF) or closely resembling tissue-resident macrophages (M-CSF).

Enrichment of CD11b cell subpopulations of bone marrow was carried out as described previously [36]. In brief, after treatment with FcR Blocking Reagent (Miltenyi Biotec), bone marrow-derived cells were stained with anti-mouse CD11b conjugated with PE (clone M1/70, BioLegend, San Diego, CA), followed by washing and incubation with anti-PE microbeads (Miltenyi Biotec). The labeled cells were passed through MS separation columns that had been equilibrated with dilution buffer. Columns were washed three times with 3 ml dilution buffer. The retained CD11b cells were eluted from the column and analyzed for CD11b surface expression by flow cytometry.

2.9. Western blotting

To determine the expression of ErbB receptors in myeloid cells, immunomagnetically sorted bone marrow CD11b positive cells (5×10^7 cells) were lysed in radioimmunoprecipitation assay (RIPA) buffer containing protease inhibitor cocktails (Roche Diagnostics, Indianapolis, IN). Total protein concentrations were quantified with the Pierce BCA Protein Assay Kit (Thermo Fisher Scientific), and resolved by 8% SDS-PAGE. After blotting, the membrane was probed with rabbit monoclonal antibodies raised against ErbB1 (D38B1), ErbB2 (29D8), ErbB3 (D22C5), or ErbB4 (111B2). All antibodies are purchased from Cell Signaling Technology (Danvers, MA).

For analysis of intramyocardial levels of NRG-1, phosphorylated IGF-1R and total IGF-1R, perfused and isolated hearts were homogenized in RIPA buffer (100 mg of heart tissue per 1000 ul of RIPA buffer). Goat polyclonal anti-NRG-1 antibody (C-18), mouse monoclonal anti-phospho-IGF-1R (2B9), and IGF-1R (7G11) antibodies were used to detect levels of NRG-1, and phosphorylation of IGF-1 receptors after TAC. All antibodies are purchased

Author Manuscript Author Manuscript Author Manuscript Author Manuscript

from Santa Cruz Biotechnology, Inc (Dallas, TX). The level of NRG-1 was normalized to the level of β-actin, which was detected using mouse monoclonal β-actin antibody (ab8224, Abcam).

Secondary peroxidase-conjugated antibodies (BioRad, Hercules, CA) and ProSignal™ Pico enhanced chemiluminescence kit (Genesee Scientific, San Diego, CA) were used for visualization, of immunoreactive bands. Densitometric analysis was conducted using ImageJ 1.45s software (NIH).

2.10. Transwell migration assay

Cell migration was evaluated using Corning® HTS Transwell® 96 well permeable supports (5.0 μm membrane pore size). Magnetically purified bone marrow CD11b cells were resuspended in 10% FBS RPMI-1640 medium and added inside the inserts at the concentration of 10^5 cells/well. The inserts were placed over wells with 10% FBS RPMI-1640 medium containing 50 ng/ml of recombinant human NRG-1 or PBS (control). After incubation under a humidified atmosphere of air/CO2 (19: 1) at 37°C for incubated for different time intervals (5, 30, 60, and 120 min), medium from the wells were collected and centrifuged at 200 x g for 5 min. Cells in the pellet were stained with 2 μM calcein–acetoxymethyl ester (Life Technologies). Fluorescence of cells was measured at excitation and emission wavelengths of 485 and 535 nm, respectively, and cell migration was calculated using a calibration curve constructed for each experiment by measuring the fluorescence of predetermined numbers of labeled cells.

2.11. Quantitative antibody array

Expression of cytokines and growth factors in mouse hearts was analyzed on day 3 post-TAC. In brief, mouse hearts (90-120 mg) were perfused with a phosphate-buffered solution to remove blood, isolated and homogenized in 1 ml of radioimmunoprecipitation assay buffer (RIPA buffer). Tissue homogenate was centrifuged at 10,000 x g for 30 min, and the supernatant was used for the analysis. A Quantibody® Mouse Cytokine Antibody Array 4000 (#QAM-CAA-4000) was conducted by RayBioTech (Norcross, GA).

2.12. Statistical analysis

Kolmogorov-Smirnov test was used as a test for normality. Normally distributed variables are expressed as mean±SEM. Comparisons between 2 groups were performed using two-tailed unpaired *t* tests. Paired *t* test was used to determine statistical significance before and after TAC. Comparisons between ≥3 groups were performed using ordinary one-way ANOVA with Tukey's multiple-comparisons post-test. The Mantel-Cox log-rank test was used to compare the survival rates in mice with ErbB3 deletion and control animals. $P<0.05$ was considered significant.

Author Manuscript Author Manuscript Author Manuscript Author Manuscript

3. RESULTS

3.1. Myeloid cell-specific ablation of ErbB3 gene expression did not alter the number of CD11b myeloid cells in circulation or their accumulation in the heart.

To compare the levels of ErbB receptors expression between ErbB3^{MyeWT} mice and ErbB3^{MyeWT} control animals, we first isolated CD11b positive cells from the primary source of myeloid cells, bone marrow (Figure 1A). We then performed the analysis of all four ErbB receptors expression using western blotting. As shown in Figure 1B, only ErbB3 and ErbB4 but not ErbB1 or ErbB2 receptors are expressed in bone marrow myeloid cells. The level of ErbB3 protein was decreased by approximately 80% in cells obtained from ErbB3^{myeKO} compared to ErbB3^{myeWT} mice (Figure 1C). It should be noted that approximately 20%-40% of CD11b positive cells in the bone marrow do not express LysM-Cre [37, 38], which explains the presence of immunoreactivity bands corresponding to ErbB3 protein in LysM-Cre-driven ErbB3 flox/flox mice. The total level of ErbB4 receptors was also decreased in knockout mice, though to a lesser degree compared to ErbB3. Because ErbB3 and ErbB4 receptors are targeted for proteasomal degradation in the endoplasmatic reticulum, it is important to determine their expression at the cell surface. Data from flow cytometric analysis of bone marrow CD11b myeloid cells revealed the down-regulation of ErbB3 cell surface expression (Figures 1D and E), confirming data from western blot analysis. No differences were found in the expression of ErbB4 at the CD11b cell surface between knockout and control animals. These data may indicate the presence of cooperation between post-translational mechanisms involved in the degradation and recycling of ErbB3 and ErbB4[39, 40].

To further characterize the expression of ErbB3 and ErbB4, we incubated Lin-hematopoietic progenitor cells in the presence of GM-CSF. Our data showed that the level of ErbB3 is significantly decreased in mature proinflammatory myeloid cells, including macrophages and monocyte-derived dendritic cells (Figures 1F and G). No differences were found in the level of cell surface expression of ErbB4.

As shown in Figures 1H, I and J, ErbB3 and ErbB4 receptors are expressed on murine myeloid cells in blood, spleen, and heart in control animals. The mean fluorescence intensity corresponding to ErbB3 receptor expression was higher on cardiac myeloid cells compared to cells in blood and spleen, suggesting the presence of factors that promote cell-surface expression of ErbB3 in cardiac tissue. Deletion of ErbB3 gene expression in myeloid cells of LysM-Cre/ErbB3 flox/flox mice resulted in the down-regulation of cell-surface expression of ErbB3 receptors. Flow cytometric analysis revealed the absence of changes in the number of CD11b/CD45 myeloid cells between control and knockout mice in all tested tissues (Figure 1K), indicating that ErbB3 receptors are not involved in myeloid cell trafficking in a steady-state condition.

3.2. ErbB3 deletion in myeloid cells is associated with an increase in body weight but no changes in cardiac function.

We found that both male and female ErbB3^{MyeKO} mice were significantly heavier than the control mice (Figure 2A). Weight gain was relatively small: approximately 25% increase in

Author Manuscript Author Manuscript Author Manuscript Author Manuscript

male and 20% increase in female body weight. NMR analysis revealed significant differences in the body fat mass and body adiposity index in knockout mice compared to control in both male (Figure 2B) and female (Figure 2C) animals. Echocardiographic evaluation revealed no changes in the left ventricular fractional shortening, indicating that the deletion of ErbB3 expression in myeloid cells did not induce changes in heart function (Figure 2D). We did, however, see an increase in the end-systolic and end-diastolic diameters, reflecting a physiological adaptation of the cardiovascular system to increased body weight in mice with myeloid cell-specific deletion of ErbB3 (Figures 2E and F). Accordingly, no differences were found in heart-to-body weight ratios in both male and female knockout mice compared to control animals (Figure 2G).

3.3. The deletion of ErbB3 expression in myeloid cells is associated with increased mortality in male mice after TAC.

We examined the effect of pressure overload on the survival of control and ErbB3 knockout mice using transverse aortic banding. While no differences were found in sham-operated mice, TAC was associated with a trend toward increased mortality in ErbB3^{MyeKO} mice compared to control animals (Figure 3A). Further analysis revealed sex-dependent differences in mice survival. TAC resulted in significantly higher mortality of male mice with ErbB3 deletion, with the median value of mice survival at day 5 after the surgery, compared to male control animals, which clearly survived longer (Figure 3B).

Interestingly, the first week after the surgery was also associated with elevated mortality in female mice with the ablation of ErbB3 expression. However, no statistical differences in the mortality rates were found between the groups of control and ErbB3^{MyeKO} female mice over the entire course of the study (Figure 3C). We estimate that the sample size needed to reach a conclusion in female mice with 85% confidence would require an additional 120 mice.

No differences were found in the pressure gradient between wild type and knockout animals (Figure 3D). Post-mortem examination of mice that died after TAC revealed an increased lung-to-body weight ratio with a mean value of 10.6 ±0.8 (n=8) in mice with ErbB3 deletion, indicating the presence of pulmonary edema, consistent with acute heart failure. To evaluate differences between control and ErbB3^{MyeKO} mice, we performed an analysis of lung-to-body weight ratios on day 3 post-TAC before the increased death of mice with ErbB3 deletion. We found that TAC surgery resulted in a significantly increased lung-to-body weight ratio in knockout male mice compared to control male animals (Figure 3E). No differences were found in the lung-to-body weight ratio between control and knockout groups of female mice (Figure 3F).

Echocardiographic assessment of cardiac function on day 3 post-TAC did not reveal significant changes in fractional shortening (Figure 3G). However, a substantial decrease in heart rate was found in knockout male mice on day 3 post-TAC compared to baseline (Figures 3H and I). The immunohistochemical analysis did not show any differences in the size of cardiomyocytes (Figures 3J and K), tissue fibrosis (Figure 3L), or number of cells that are positive for cleaved caspase-3 (Figure 3M, apoptotic cells) between knockout and wild type animals on day 3 post-TAC.

Author Manuscript Author Manuscript Author Manuscript Author Manuscript

3.4. Deletion of ErbB3 receptors results in the lower accumulation of CD11b myeloid cells in male mice after TAC.

To determine whether the deletion of ErbB3 resulted in the altered immune response to pressure overload, we performed flow cytometric characterization of cell suspensions obtained from hearts of control and ErbB3^{MyeKO} mice on day 3 post-TAC. Since the expression of ErbB3 was disrupted in myeloid cells, we first evaluated populations of CD11b and CD45 positive cells. We found that TAC induces an increase in the percentages and numbers of CD11b myeloid cells and CD45 immune cells in the hearts of both control and male knockout mice (Figures 4A-C). However, the number of immune cells, and myeloid cells, specifically, was significantly lower in the hearts of ErbB3^{MyeKO} mice compared to the control group. Further analysis revealed that the majority of CD11b positive cells infiltrating the heart of mice after the surgery were Ly6G neutrophils and Ly6C monocytes (Figures 4D and E). The accumulation of both of these subpopulations was significantly reduced in male mice with ErbB3 deletion compared to control animals.

Similar to the effect in male mice, TAC surgery induces the accumulation of myeloid cells in the hearts of female mice (Figure 4F-J). However, in contrast to male mice, no differences in the numbers of infiltrating CD11b/CD45 positive cells or subpopulations of neutrophils and monocytes were found between the groups of control and ErbB3^{MyeKO} female mice.

3.5. ErbB3 promotes the migration of myeloid cells.

To elucidate the effect of ErbB3 signaling on myeloid cell migration, we analyzed cell migration *in vitro* using a transwell system. We used purified CD11b positive myeloid cells from murine bone marrow to determine the effect of the recombinant extracellular domain of neuregulin-1 (active form) on cells obtained from control animals with intact ErbB3 signaling. We found that neuregulin-1 promotes the migration of CD11b cells. The effect of neuregulin-1 reached a peak at one hour after the initiation of migration (Figure 5A). To further characterize the migration, we analyzed cells in the two chambers of a transwell system and found that only CD11b positive cells migrated from the upper to lower chamber (Figure 5B). Next, we analyzed the effect of neuregulin-1 on myeloid cells isolated from male and female mice separately. Deletion of ErbB3 resulted in the abolishment of the effect of neuregulin-1 on the migration of CD11b positive myeloid cells from both male and female mice (Figures 5C and D).

To determine whether the level of ErbB receptor ligands is changing in the hearts after the aortic banding, we performed Western blot analysis of neuregulin-1, an ErbB3 ligand. As shown in Figures 5 E and F, the low molecular neuregulin-1 (extracellular domain, active form) is increased on day 3 post-TAC in both wild type and knockout animals compared to the basal (pre-operative) level. These data indicate that neuregulin-1/ ErbB3 signaling promotes CD11b cell migration and that an increased level of intramyocardial neuregulin-1 is involved in the accumulation of myeloid cells after TAC.

Author Manuscript Author Manuscript Author Manuscript Author Manuscript

3.6. TAC induces the proliferation of Sca-1 positive non-immune cells in control but not ErbB3^{MyeKO} male mice.

To better characterize the effect of TAC in control mice and animals with the deletion of ErbB3, we investigated the composition of non-immune cells using flow cytometry. We found that the percent of Sca-1 positive non-immune (CD45 negative) cells was increased on day 3 post-TAC in control animals (Figure 6A). No difference, however, was found in cell suspensions obtained from the hearts of ErbB3^{MyeKO} male mice.

In the murine heart, Sca-1 is expressed on endothelial cells, fibroblasts[41, 42], and mesenchymal cells with pro-angiogenic signaling [33]. We found that the number of endothelial cells, as well as Sca-1^{pos}/CD31^{neg} fibroblasts, was higher on day 3 post-TAC compared to basal level (before surgery) in the control mice (Figure 6B and C). These changes did not reach statistical significance in male ErbB3^{MyeKO} mice. Further analysis revealed an increased number of proliferating Sca-1 cells in control but not ErbB3^{MyeKO} mice post-TAC (Figure 6D), indicating that the increased number of Sca-1 expressing cells in control animals is due to the stimulation of their proliferation. No effects of TAC on apoptosis of Sca-1 positive cells were found during the first 3 days after the surgery (Figure 6E).

A similar analysis demonstrated that in contrast to male mice, TAC was associated with the proliferation of CD31 endothelial cells in both control and ErbB3^{MyeKO} female mice (Figure 6F and G). While we found no effect of TAC on the number of Sca-1^{pos}/CD31^{neg} cells in mice with ErbB3 deletion (Figure 6H), the total number of proliferating Sca-1 cells was higher in both groups of female mice on day 3 after the surgery (Figure 6I). The number of apoptotic cells was not increased after TAC and was similar between the groups (Figure 6J).

3.7. Mice with ErbB3 deletion are characterized by the lower level of IGF-1 expressing cells after TAC.

Myeloid cells express many cytokines and growth factors that could play a role in their stimulation of proliferation of endothelial cells and fibroblasts and in the regulation of myocyte hypertrophic response. To examine potential mechanisms by which the impaired accumulation of myeloid cells in male ErbB3^{MyeKO} mice regulates cardiac cell biology, we analyzed the level of cytokines and growth factors in the heart's lysates post-TAC using quantitative antibody array (Figure 7A). This analysis identified several differences, including the lower levels of insulin growth factor-1 (IGF-1), ADAM metallopeptidase with thrombospondin type 1 motif 1 (ADAMTS1), fetuin A, and chordin in hearts of ErbB3^{MyeKO} mice compared to control animals (Figure 7B). In contrast, the level of TNF-like weak inducer of apoptosis (TWEAK) was increased in mice with ErbB3 deletion. We also found a trend towards a higher level of prostasin, a serine protease, in ErbB3^{MyeKO} mice.

IGF-1 is a well-known factor contributing to the compensatory hypertrophic response. To validate the antibody array data and determine whether or not the decreased level of IGF-1 is associated with decreased IGF-1 signaling in the heart, we performed western blot analysis of IGF-1 receptor phosphorylation. As shown in Figures 7C and D, the level of

Author Manuscript Author Manuscript Author Manuscript Author Manuscript

phosphorylated IGF-1R was decreased in the heart lysates obtained from knockout male mice compared to control animals.

No differences were found in the level of IGF-1 in the peripheral circulation (Figure 7E), indicating that the lower level of IGF-1 in the hearts of knockout mice is not due to decreased synthesis of IGF-1 in the liver. To determine the source of IGF-1, we performed flow cytometric analysis of the intracellular level of IGF-1 in subpopulations of cardiac cells. We found that both CD11b myeloid cells and non-myeloid cells are characterized by the low level of IGF-1 production in steady-state conditions in male mice (Figure 7F). TAC was associated with an increase in the percent of IGF-1 positive cells in control mice but not in ErbB3^{MyeKO} male mice, consistent with the quantitative antibody array data. To determine what type of cells are producing IGF-1 besides CD11b myeloid cells, we performed flow cytometric analysis of CD45^{neg} non-immune cells (Figure 7G). We found that Sca-1 positive cells represent a major population of IGF-1-producing cells in both sham-operated and TAC control animals among the non-immune cardiac population. Similar to male mice, the percent of IGF-1 producing cells was lower in ErbB3^{MyeKO} female mice as compared to control mice post-TAC (Figure 7H). Calculation of flow cytometric data indicated a significant accumulation of IGF-1 producing cells (sum of myeloid and non-immune cells) in control male mice on day 3 post-TAC (Figure 7I). No differences were found in the number of IGF-1 positive cells between sham and TAC in the groups of male mice with ErbB3 deletion in myeloid cells. In contrast to male mice, aortic banding increased the number of IGF-1 producing cells in both groups of female mice on day 3 after TAC compared to sham-operated animals (Figure 7J). To determine whether loss of ErbB3 is associated with decreased production of IGF-1 from CD11b cells, we measured the level of IGF-1 in the supernatant of bone marrow-derived myeloid cells incubated in the presence of GM-CSF to generate proinflammatory macrophages and dendritic cells (Figure 7K), or M-CSF to generate cell resembling the phenotype of tissue-resident macrophages (Figure 7L). No differences were found between bone marrow-derived mature myeloid cells obtained from wild type and knockout animals in the production of IGF-1.

4. DISCUSSION

Our main findings are that myeloid cell-specific ErbB3 signaling is involved in the regulation of myeloid cell migration into the male heart after pressure overload, and that reduced accumulation of immune cells in the myocardium and is associated with a blunted proliferative response of endothelial cells and fibroblasts, and increased mortality in male mice during the first week after TAC.

Emerging evidence indicates that ErbB receptor signaling plays a role in the regulation of immune and inflammatory responses [26, 28]. In agreement with previous observations [28, 43, 44], we found the expression of ErbB3 and ErbB4 but not ErbB1 or ErbB2 in myeloid cells. Our study revealed the decrease in the total level of ErbB4 protein in ErbB3 knockout CD11b cells, which may indicate the presence of cross-talk between post-translational modification of ErbB3 and ErbB4 in myeloid cells. Interestingly, E3 ubiquitin-protein ligase NRDP1 interacts with both ErbB3 and ErbB4, targeting newly synthesized receptors for the proteasomal degradation [39, 45]. We suggest that in the absence of ErbB3, the activity of

Author Manuscript Author Manuscript Author Manuscript Author Manuscript

NRDP1 could be redirected toward ErbB4, resulting in its increased ubiquitination and proteasomal degradation. However, we did not find the down-regulation of ErbB4 expression at the cell surface. It would be interesting to investigate whether or not ErbB3 controls ErbB4 recycling [46]. Importantly, our study revealed the absence of compensatory up-regulation of other subtypes of ErbB receptors after the loss of ErbB3, indicating that ErbB3 plays a non-redundant role in myeloid cells.

In contrast to the immune response after ischemic myocardial injury [47-51], the infiltration of immune cells and their role after non-ischemic heart injury remain to be elucidated. Recently, several studies demonstrated the early immune cell accumulation and their role in the regulation of cardiac hypertrophic response using a mouse model of pressure overload-induced left ventricular hypertrophy and heart failure [14, 17, 52]. Interestingly, the experiments with relatively late, two weeks after aortic banding, depletion of Ly6C^{high} monocytes, and proinflammatory macrophages demonstrated that these cells are dispensable for progression to remodeling and failure, indirectly pointing toward the specific contribution of mononuclear phagocytes in early compensatory response[16]. In agreement with these studies, we found rapid accumulation, within the first three days, of CD45 positive immune cells in the heart after aortic banding in mice with intact ErbB3 signaling in myeloid cells. Flow cytometric analysis demonstrated that the majority of immune cells were represented by CD11b positive myeloid cells, including Ly6G neutrophils and Ly6C^{high} monocytes.

One major finding of the current investigation is that mice with myeloid cell-specific deletion of ErbB3 demonstrated sex-specific differences characterized by a significantly decreased accumulation of myeloid cells in the hearts of male mice. One potential explanation of the impaired immune response in ErbB3 knockout mice might be related to the contribution of ErbB3 signaling to cell migration. The role of NRG-1/ErbB signaling in the migration of non-immune cells [53-56], as well as the migration of lymphocytes[57] and primary immune cells[58] of the central nervous system, has been shown previously. In our study, we demonstrated for the first time that NRG-1 stimulated the migration of bone marrow myeloid cells *in vitro* via activation of ErbB3. This finding explains the reduced accumulation of myeloid cells found in male mice with ErbB3 deletion. While we do not have an explanation of unaffected intramyocardial accumulation of immune cells in female knockout mice, we speculate that the relative contribution of ErbB3 signaling in the migration of myeloid cells *in vivo* might be different between male and female mice. Sex hormones are involved in the regulation of immune response [59-61]. Cross-talk between ErbB and estrogen receptors [62] or androgen receptors [63] may be responsible for differences found between male and female mice. Sex steroid hormone receptors are expressed at different levels on mononuclear phagocytes from men and women [64]. Sex differences are associated with variances in the immune response to infection and heart injury in clinical myocarditis, with males having worse outcomes than females [65, 66]. Further studies are warranted to investigate interactions between ErbB3 and sex hormone receptors in the regulation of myeloid cell migration.

The second major finding relates to increased early mortality in male mice with myeloid cell-specific deletion of ErbB3. Transverse aortic constriction is associated with a low mortality rate, rarely exceeding twenty percent in the first two weeks after surgery, the time

Author Manuscript Author Manuscript Author Manuscript Author Manuscript

required for the development of compensatory response[12, 67]. However, modifications of genes that contribute to the development of compensatory responses may lead to significantly increased mouse mortality early after TAC [68-70]. There are a limited number of studies showing the involvement of immune cells in the adaptive response to elevated afterload. Meguro et al [71] demonstrated that compensatory hypertrophic growth is attenuated by cyclosporine and associated with enhanced susceptibility to decompensation, heart failure, and increased mortality within the first ten days after TAC. While the authors did not examine the immune response, the well-known immunosuppressive effects of cyclosporine, including inhibition of myeloid cell migration [72-74], implicates a role for immune cells in the early compensatory response post-TAC.

A recent study demonstrated an important role played by cardiac resident macrophages in the early adaptive response to TAC. Liao et al[15] found that hemodynamic overload-induced macrophage proliferation was followed by cardiac accumulation of macrophages on day 7 after the surgery. Clodronate-mediated depletion of mononuclear phagocytes was associated with ~80% mouse mortality within six days after TAC. Since no effect of CCR2 antagonist was found, the authors concluded that resident cardiac macrophages but not blood monocytes are involved in the development of compensatory cardiac response. We found a similarly high mortality phenotype in male mice with ErbB3 deletion and significantly reduced infiltration of neutrophils and monocytes. Our findings indicate the presence of complex interactions between neutrophils, monocytes, and resident macrophages, during an early adaptive response. Neutrophils are known to induce proliferation of macrophages[75, 76], and early accumulation of neutrophils after TAC may provide the signals for macrophage proliferation and macrophage-dependent cardiomyocyte protection[77].

Although the cause of animal death in the absence of intramyocardial accumulation of myeloid cells is not known, both Liao et al[15] and our current study demonstrate the presence of pulmonary edema at day 4 and day 3 post-TAC, respectively. Pulmonary edema often develops in parallel with dilated cardiomyopathy in the pressure overload model [78]. However, no changes in fractional shortening were found in ErbB3 knockout animals, indicative of preserved systolic function. Diastolic dysfunction is also associated with pulmonary edema [79-82]. While we did not evaluate diastolic function in this study, several factors point in this direction, including a moderate obesity phenotype [83-85] and low myocardial IGF-1 level in knockout animals [86, 87]. In addition, low heart rate, found in myeloid cell-specific ErbB3 knockout male mice may indicate a potential disturbance in the cardiac conduction system. It has been recently shown that cardiac macrophages are involved in facilitating electrical conduction [88]. Further studies are necessary to determine whether or not ErbB3 signaling in myeloid cells is involved in the regulation of the electrical conduction system or diastolic function in stressed myocardium.

Another important aspect of our work is related to the role of myeloid cells in the proliferation of cardiac mesenchymal cells after TAC. The early induction of endothelial cell proliferation in response to pressure overload has been previously documented [89]. In the current study, we found that aortic banding induced proliferation of Sca-1 expressing mesenchymal cells. These cells are represented by subpopulations of endothelial cells and non-endothelial cells with pro-angiogenic properties [33, 90]. Angiogenesis is necessary for an

Author Manuscript Author Manuscript Author Manuscript Author Manuscript

adaptive response to hemodynamic overload, and the imbalance between the growth of cardiomyocytes and angiogenesis results in contractile dysfunction and heart failure [91, 92]. It has been recently demonstrated that physiological cardiomyocyte growth is regulated by VEGF/VEGFR2-dependent signaling, which induces ADAM12 and KLK8-mediated shedding of NRG-1 from endothelial cells [93]. The transient upregulation of VEGF expression has been found early, on day 1, after TAC [94]. Interestingly, we found an increase in the level of NRG-1 protein on day 3 after TAC, pointing toward the activation of VEGF/VEGFR2/ADAM12/NRG-1 signaling axis in response to increased cardiac afterload. The absence of Sca-1 cell proliferation in male knockout mice demonstrated an important role of myeloid cell-specific ErbB3 signaling, which connects cardiac mesenchymal cells activation with early immune response contributing to angiogenesis. Our data also suggest that the upregulation of IGF-1 may represent an important mechanistic link between immune accumulation and angiogenesis[95, 96] in response to cardiac overload.

Previous studies demonstrated that monocytes and macrophages represent a source of IGF-1 [97-100]. In agreement with these studies, we also found that infiltrating CD11b myeloid cells are characterized by increased production of IGF-1. Additionally, our data demonstrated that Sca-1 mesenchymal cells produce IGF-1 and that the production of IGF-1 is upregulated after TAC. However, this effect is most likely dependent on myeloid cell infiltration in the heart since no differences were found in the production of IGF-1 by myeloid cells from wild type and knockout animals, and no effect of aortic banding was found on the production of IGF-1 by Sca-1 cells in male mice with reduced accumulation of CD11b cells.

In summary, our current study demonstrated for the first time that ErbB3 signaling in myeloid cells plays a crucial role in sex-specific adaptation to increased hemodynamic loading. Activation of ErbB3 promotes early accumulation of neutrophils and monocytes in pressure overload stressed myocardium in male mice. Myeloid cells induce endothelial cells and fibroblasts expansion and activation, which in turn, promotes early compensatory response through the production of IGF-1[101] and protection of cardiac function[87, 102, 103]. We have previously shown that the expression of ErbB3 is characterized by large inter-individual variability in human myeloid cells [28]. Our current finding on the role of ErbB3 signaling provides a better understanding of differences seen in disease progression in patients with heart failure and highlights the importance of studies focused on the role of myeloid cells in cardiovascular diseases.

ACKNOWLEDGMENTS

We are grateful to Dr. Volkhard Lindner, Grazina Armie Mangoba and the Histopathology Core, for help with tissue processing and Immunohistochemical staining. Graphical abstract was created with BioRender.com

SOURCES OF FUNDING

This work was supported by the Maine Medical Center Cardiovascular Research Institute 2015 Pilot Project Program, the National Heart, Lung, and Blood Institute of the National Institutes of Health under grants U01 HL100398, R01 HL136560, R01 HL139887, and the American Heart Association under grant 17POST33410474. We utilized Maine Medical Center's Progenitor Cell Analysis Core facility which is supported by NIH/NIGMS grants P30GM106391, COBRE in Stem and Progenitor Cell Biology and Regenerative Medicine, and U54GM115516, Northern New England Clinical and Translational Research Network (Translational Technologies Core). The content is solely the responsibility of the authors and does not necessarily represent the official views of the National Institutes of Health.

Author Manuscript Author Manuscript Author Manuscript Author Manuscript

REFERENCES

1. Benjamin EJ, Muntner P, Alonso A, Bittencourt MS, Callaway CW, Carson AP, Chamberlain AM, Chang AR, Cheng S, Das SR, Delling FN, Djousse L, Elkind MSV, Ferguson JF, Fornage M, Jordan LC, Khan SS, Kissela BM, Knutson KL, Kwan TW, Lackland DT, Lewis TT, Lichtman JH, Longenecker CT, Loop MS, Lutsey PL, Martin SS, Matsushita K, Moran AE, Mussolino ME, O'Flaherty M, Pandey A, Perak AM, Rosamond WD, Roth GA, Sampson UKA, Satou GM, Schroeder EB, Shah SH, Spartano NL, Stokes A, Tirschwell DL, Tsao CW, Turakhia MP, VanWagner LB, Wilkins JT, Wong SS and Virani SS. Heart Disease and Stroke Statistics—2019 Update: A Report From the American Heart Association. 2019;139:e56–e528.
2. Mehta J, Dinerman J, Mehta P, Saldeen TG, Lawson D, Donnelly WH and Wallin R. Neutrophil function in ischemic heart disease. 1989;79:549–556.
3. Apostolakis S, Lip GYH and Shantsila E. Monocytes in heart failure: relationship to a deteriorating immune overreaction or a desperate attempt for tissue repair? Cardiovascular research. 2009;85:649–660. [PubMed: 19805399]
4. Frantz S and Nahrendorf M. Cardiac macrophages and their role in ischaemic heart disease. Cardiovascular research. 2014;102:240–248. [PubMed: 24501331]
5. Bansal SS, Ismahil MA, Goel M, Zhou G, Rokosh G, Hamid T and Prabhu SD. Dysfunctional and Proinflammatory Regulatory T-Lymphocytes Are Essential for Adverse Cardiac Remodeling in Ischemic Cardiomyopathy. Circulation. 2019; 139:206–221. [PubMed: 30586716]
6. Meng X, Yang J, Dong M, Zhang K, Tu E, Gao Q, Chen W, Zhang C and Zhang Y. Regulatory T cells in cardiovascular diseases. Nature Reviews Cardiology. 2016;13:167–179. [PubMed: 26525543]
7. Follath F Nonischemic heart failure: epidemiology, pathophysiology, and progression of disease. J Cardiovasc Pharmacol. 1999;33 Suppl 3:S31–5. [PubMed: 10442682]
8. Yildiz A, Yüksel M, Oylumlu M, Polat N, Akil MA and Acet H. The association between the neutrophil/lymphocyte ratio and functional capacity in patients with idiopathic dilated cardiomyopathy. Anatol J Cardiol. 2015;15:13–17. [PubMed: 25179880]
9. Rudolph V, Rudolph TK, Hennings JC, Blankenberg S, Schnabel R, Steven D, Haddad M, Knittel K, Wende S, Wenzel J, Münzel T, Heitzer T, Meinertz T, Hübner C and Baldus S. Activation of polymorphonuclear neutrophils in patients with impaired left ventricular function. Free Radical Biology and Medicine. 2007;43:1189–1196. [PubMed: 17854714]
10. Huber KC, Gersh BJ, Sugrue DD, Frye RL, Bailey KR and Ritts RE Jr. T-lymphocyte subsets in patients with idiopathic dilated cardiomyopathy. International journal of cardiology. 1989;22:59–66. [PubMed: 2564379]
11. deAlmeida AC, van Oort RJ and Wehrens XH. Transverse aortic constriction in mice. J Vis Exp. 2010.
12. Frey N, Katus Hugo A, Olson Eric N and Hill Joseph A. Hypertrophy of the Heart. Circulation. 2004; 109:1580–1589. [PubMed: 15066961]
13. Xia Y, Lee K, Li N, Corbett D, Mendoza L and Frangogiannis NG. Characterization of the inflammatory and fibrotic response in a mouse model of cardiac pressure overload. Histochemistry and cell biology. 2009; 131:471–481. [PubMed: 19030868]
14. Patel B, Bansal SS, Ismahil MA, Hamid T, Rokosh G, Mack M and Prabhu SD. CCR2(+) Monocyte-Derived Infiltrating Macrophages Are Required for Adverse Cardiac Remodeling During Pressure Overload. JACC Basic Transl Sci. 2018;3:230–244. [PubMed: 30062209]
15. Liao X, Shen Y, Zhang R, Sugi K, Vasudevan NT, Alaiti MA, Sweet DR, Zhou L, Qing Y, Gerson SL, Fu C, Wynshaw-Boris A, Hu R, Schwartz MA, Fujioka H, Richardson B, Cameron MJ, Hayashi H, Stamler JS and Jain MK. Distinct roles of resident and nonresident macrophages in nonischemic cardiomyopathy. Proceedings of the National Academy of Sciences of the United States of America. 2018;115:E4661–E4669. [PubMed: 29712858]
16. Patel B, Ismahil MA, Hamid T, Bansal SS and Prabhu SD. Mononuclear Phagocytes Are Dispensable for Cardiac Remodeling in Established Pressure-Overload Heart Failure. PloS one. 2017;12:e0170781. [PubMed: 28125666]

Author Manuscript Author Manuscript Author Manuscript Author Manuscript

17. Wang Y, Sano S, Oshima K, Sano M, Watanabe Y, Katanasaka Y, Yura Y, Jung C, Anzai A, Swirski FK, Gokce N and Walsh K. Wnt5a-Mediated Neutrophil Recruitment Has an Obligatory Role in Pressure Overload–Induced Cardiac Dysfunction. 2019;140:487–499.

18. Laroumanie F, Douin-Echinard V, Pozzo J, Lairez O, Tortosa F, Vinel C, Delage C, Calise D, Dutaur M, Parini A and Pizzinat N. $CD4^+$ T Cells Promote the Transition From Hypertrophy to Heart Failure During Chronic Pressure Overload. 2014;129:2111–2124.

19. Kallikourdis M, Martini E, Carullo P, Sardi C, Roselli G, Greco CM, Vignali D, Riva F, Ormbostad Berre AM, Stølen TO, Fumero A, Faggian G, Di Pasquale E, Elia L, Rumio C, Catalucci D, Papait R and Condorelli G. T cell costimulation blockade blunts pressure overload-induced heart failure. Nature communications. 2017;8:14680–14680.

20. Fuller SJ, Sivarajah K and Sugden PH. ErbB receptors, their ligands, and the consequences of their activation and inhibition in the myocardium. Journal of molecular and cellular cardiology. 2008;44:831–54. [PubMed: 18430438]

21. Odiete O, Hill Mf and Sawyer DB. Neuregulin in cardiovascular development and disease. Circulation research. 2012;111:1376–85. [PubMed: 23104879]

22. Higashiyama S, Iwabuki H, Morimoto C, Hieda M, Inoue H and Matsushita N. Membrane-anchored growth factors, the epidermal growth factor family: beyond receptor ligands. Cancer science. 2008;99:214–20. [PubMed: 18271917]

23. Galindo CL, Ryzhov S and Sawyer DB. Neuregulin as a heart failure therapy and mediator of reverse remodeling. Current heart failure reports. 2014;11:40–9. [PubMed: 24234399]

24. Milillo MA, Velásquez LN, Trotta A, Delpino MV, Marinho FV, Balboa L, Vermeulen M, Espindola SL, Rodriguez-Rodrigues N, Fernández GC, Oliveira SC, Giambartolomei GH and Barrionuevo P. B. abortus RNA is the component involved in the down-modulation of MHC-I expression on human monocytes via TLR8 and the EGFR pathway. PLoS pathogens. 2017;13:e1006527–e1006527. [PubMed: 28767704]

25. Platen C, Dreschers S, Reiss LK, Wappler J and Orlikowsky TW. Amphiregulin Regulates Phagocytosis-Induced Cell Death in Monocytes via EGFR and Matrix Metalloproteinases. Mediators of inflammation. 2018;2018:4310419–4310419. [PubMed: 30524196]

26. Schumacher MA, Hedl M, Abraham C, Bernard JK, Lozano PR, Hsieh JJ, Almohazey D, Bucar EB, Punit S, Dempsey PJ and Frey MR. ErbB4 signaling stimulates pro-inflammatory macrophage apoptosis and limits colonic inflammation. Cell Death Dis. 2017;8:e2622–e2622. [PubMed: 28230865]

27. Vermeulen Z, Hervent A-S, Dugaucquier L, Vandekerckhove L, Rombouts M, Beyens M, Schrijvers DM, Meyer GRYD, Maudsley S, Keulenaer GWD and Segers VFM. Inhibitory actions of the NRG-1/ErbB4 pathway in macrophages during tissue fibrosis in the heart, skin, and lung. 2017;313:H934–H945.

28. Ryzhov S, Matafonov A, Galindo CL, Zhang Q, Tran TL, Lenihan DJ, Lenneman CG, Feoktistov I and Sawyer DB. ERBB signaling attenuates proinflammatory activation of nonclassical monocytes. American journal of physiology Heart and circulatory physiology. 2017;312:H907–H918. [PubMed: 28235789]

29. Qu S, Rinehart C, Wu H-H, Wang SE, Carter B, Xin H, Kotlikoff M and Arteaga CL. Gene targeting of ErbB3 using a Cre-mediated unidirectional DNA inversion strategy. genesis. 2006;44:477–486. [PubMed: 16991114]

30. Cook RS, Garrett JT, Sanchez V, Stanford JC, Young C, Chakrabarty A, Rinehart C, Zhang Y, Wu Y, Greenberger L, Horak ID and Arteaga CL. ErbB3 ablation impairs PI3K/Akt-dependent mammary tumorigenesis. Cancer research. 2011;71:3941–51. [PubMed: 21482676]

31. Richards DA, Aronovitz MJ, Calamaras TD, Tam K, Martin GL, Liu P, Bowditch HK, Zhang P, Huggins GS and Blanton RM. Distinct Phenotypes Induced by Three Degrees of Transverse Aortic Constriction in Mice. Scientific reports. 2019;9:5844. [PubMed: 30971724]

32. Li L, Guo X, Chen Y, Yin H, Li J, Doan J and Liu Q. Assessment of Cardiac Morphological and Functional Changes in Mouse Model of Transverse Aortic Constriction by Echocardiographic Imaging. J Vis Exp. 2016.

33. Ryzhov S, Goldstein AE, Novitskiy SV, Blackburn MR, Biaggioni I and Feoktistov I. Role of A2B adenosine receptors in regulation of paracrine functions of stem cell antigen 1-positive cardiac

Author Manuscript Author Manuscript Author Manuscript Author Manuscript

stromal cells. The Journal of pharmacology and experimental therapeutics. 2012;341:764–74. [PubMed: 22431204]

34. Halldorsdottir S, Carmody J, Boozer CN, Leduc CA and Leibel RL. Reproducibility and accuracy of body composition assessments in mice by dual energy x-ray absorptiometry and time domain nuclear magnetic resonance. Int J Body Compos Res. 2009;7:147–154. [PubMed: 21909234]
35. Hardy MY, Kassianos AJ, Vulink A, Wilkinson R, Jongbloed SL, Hart DN and Radford KJ. NK cells enhance the induction of CTL responses by IL-15 monocyte-derived dendritic cells. Immunology and cell biology. 2009;87:606–14. [PubMed: 19546878]
36. Ryzhov S, Novitskiy SV, Goldstein AE, Biktasova A, Blackburn MR, Biaggioni I, Dikov mM and Feoktistov I. Adenosinergic regulation of the expansion and immunosuppressive activity of CD11b +Gr1+ cells. Journal of immunology. 2011;187:6120–9.
37. McCubbrey AL, Allison KC, Lee-Sherick AB, Jakubzick CV and Janssen WJ. Promoter Specificity and Efficacy in Conditional and Inducible Transgenic Targeting of Lung Macrophages. Front Immunol. 2017;8:1618. [PubMed: 29225599]
38. Shi J, Hua L, Harmer D, Li P and Ren G. Cre Driver Mice Targeting Macrophages. Methods in molecular biology. 2018;1784:263–275. [PubMed: 29761406]
39. Diamonti AJ, Guy PM, Ivanof C, Wong K, Sweeney C and Carraway KL 3rd. An RBCC protein implicated in maintenance of steady-state neuregulin receptor levels. Proceedings of the National Academy of Sciences of the United States of America. 2002;99:2866–71. [PubMed: 11867753]
40. Sorkin A and Goh LK. Endocytosis and intracellular trafficking of ErbBs. Experimental cell research. 2008;314:3093–106. [PubMed: 18793634]
41. Pinto Alexander R, Ilinykh A, Ivey Malina J, Kuwabara Jill T, D'Antoni Michelle L, Debuque R, Chandran A, Wang L, Arora K, Rosenthal Nadia A and Tallquist Michelle D. Revisiting Cardiac Cellular Composition. Circulation research. 2016; 118:400–409. [PubMed: 26635390]
42. Lee RT. Adult Cardiac Stem Cell Concept and the Process of Science. Circulation. 2018; 138:2940–2942. [PubMed: 30566005]
43. Wang H, Jin Y, Reddy MV, Podolsky R, Liu S, Yang P, Bode B, Reed JC, Steed RD, Anderson SW, Steed L, Hopkins D, Huang Y and She JX. Genetically dependent ERBB3 expression modulates antigen presenting cell function and type 1 diabetes risk. PloS one. 2010;5:e11789. [PubMed: 20668683]
44. Xu G, Watanabe T, Iso Y, Koba S, Sakai T, Nagashima M, Arita S, Hongo S, Ota H, Kobayashi Y, Miyazaki A and Hirano T. Preventive Effects of Heregulin-β1 on Macrophage Foam Cell Formation and Atherosclerosis. Circulation research. 2009;105:500–510. [PubMed: 19644050]
45. Fry WH, Simion C, Sweeney C and Carraway KL 3rd. Quantity control of the ErbB3 receptor tyrosine kinase at the endoplasmic reticulum. Molecular and cellular biology. 2011;31:3009–18. [PubMed: 21576364]
46. Sundvall M, Korhonen A, Paatero I, Gaudio E, Melino G, Croce CM, Aqeilan RI and Elenius K. Isoform-specific monoubiquitination, endocytosis, and degradation of alternatively spliced ErbB4 isoforms. Proceedings of the National Academy of Sciences of the United States of America. 2008;105:4162–7. [PubMed: 18334649]
47. Dewald O, Zymek P, Winkelmann K, Koerting A, Ren G, Abou-Khamis T, Michael LH, Rollins BJ, Entman ML and Frangogiannis NG. CCL2/Monocyte Chemoattractant Protein-1 regulates inflammatory responses critical to healing myocardial infarcts. Circulation research. 2005;96:881–9. [PubMed: 15774854]
48. Frangogiannis NG. The inflammatory response in myocardial injury, repair, and remodelling. Nature reviews Cardiology. 2014;11:255–65. [PubMed: 24663091]
49. Ong SB, Hernandez-Resendiz S, Crespo-Avilan GE, Mukhametshina RT, Kwek XY, Cabrera-Fuentes HA and Hausenloy DJ. Inflammation following acute myocardial infarction: Multiple players, dynamic roles, and novel therapeutic opportunities. Pharmacol Ther. 2018;186:73–87. [PubMed: 29330085]
50. Nahrendorf M, Swirski FK, Aikawa E, Stangenberg L, Wurdinger T, Figueiredo JL, Libby P, Weissleder R and Pittet MJ. The healing myocardium sequentially mobilizes two monocyte subsets with divergent and complementary functions. The Journal of experimental medicine. 2007;204:3037–47. [PubMed: 18025128]

Author Manuscript Author Manuscript Author Manuscript Author Manuscript

51. van der Laan AM, Nahrendorf M and Piek JJ. Healing and adverse remodelling after acute myocardial infarction: role of the cellular immune response. Heart. 2012;98:1384–90. [PubMed: 22904145]
52. Weisheit C, Zhang Y, Faron A, Köpke O, Weisheit G, Steinsträsser A, Frede S, Meyer R, Boehm O, Hoeft A, Kurts C and Baumgarten G. Ly6C(low) and not Ly6C(high) macrophages accumulate first in the heart in a model of murine pressure-overload. PloS one. 2014;9:e112710–e112710. [PubMed: 25415601]
53. Perlin JR, Lush ME, Stephens WZ, Piotrowski T and Talbot WS. Neuronal Neuregulin 1 type III directs Schwann cell migration. Development. 2011;138:4639–48. [PubMed: 21965611]
54. Ortega MC, Bribian A, Peregrin S, Gil MT, Marin O and de Castro F. Neuregulin-1/ErbB4 signaling controls the migration of oligodendrocyte precursor cells during development. Exp Neurol. 2012;235:610–20. [PubMed: 22504067]
55. Haskins JW, Nguyen DX and Stern DF. Neuregulin 1–activated ERBB4 interacts with YAP to induce Hippo pathway target genes and promote cell migration. Science Signaling. 2014;7:ra116. [PubMed: 25492965]
56. Jumper N, Hodgkinson T, Paus R and Bayat A. A Role for Neuregulin-1 in Promoting Keloid Fibroblast Migration via ErbB2-mediated Signaling. Acta Derm Venereol. 2017;97:675–684. [PubMed: 27882385]
57. Sei Y, Ren-Patterson R, Li Z, Tunbridge EM, Egan MF, Kolachana BS and Weinberger DR. Neuregulin1-induced cell migration is impaired in schizophrenia: association with neuregulin1 and catechol-o-methyltransferase gene polymorphisms. Molecular Psychiatry. 2007; 12:946–957. [PubMed: 17440436]
58. Calvo M, Zhu N, Tsantoulas C, Ma Z, Grist J, Loeb JA and Bennett DL. Neuregulin-ErbB signaling promotes microglial proliferation and chemotaxis contributing to microgliosis and pain after peripheral nerve injury. The Journal of neuroscience : the official journal of the Society for Neuroscience. 2010;30:5437–50. [PubMed: 20392965]
59. Gubbels Bupp MR and Jorgensen TN. Androgen-Induced Immunosuppression. Front Immunol. 2018;9:794. [PubMed: 29755457]
60. Taneja V Sex Hormones Determine Immune Response. Front Immunol. 2018;9:1931. [PubMed: 30210492]
61. Bereshchenko O, Bruscoli S and Riccardi C. Glucocorticoids, Sex Hormones, and Immunity. Front Immunol. 2018;9:1332. [PubMed: 29946321]
62. Sonne-Hansen K, Norrie IC, Emdal KB, Benjaminsen RV, Frogne T, Christiansen IJ, Kirkegaard T and Lykkesfeldt AE. Breast cancer cells can switch between estrogen receptor α and ErbB signaling and combined treatment against both signaling pathways postpones development of resistance. Breast Cancer Research and Treatment. 2010;121:601–613. [PubMed: 19697122]
63. Muniyan S, Chen SJ, Lin FF, Wang Z, Mehta PP, Batra SK and Lin MF. ErbB-2 signaling plays a critical role in regulating androgen-sensitive and castration-resistant androgen receptor-positive prostate cancer cells. Cell Signal. 2015;27:2261–71. [PubMed: 26257301]
64. McCrohon JA, Death AK, Nakhla S, Jessup W, Handelsman DJ, Stanley KK and Celermajer DS. Androgen Receptor Expression Is Greater in Macrophages From Male Than From Female Donors. 2000;101:224–226.
65. Fairweather D, Cooper LT Jr. and Blauwet LA. Sex and gender differences in myocarditis and dilated cardiomyopathy. Curr Probl Cardiol. 2013;38:7–46. [PubMed: 23158412]
66. Jin JM, Bai P, He W, Wu F, Liu XF, Han DM, Liu S and Yang JK. Gender Differences in Patients With COVID-19: Focus on Severity and Mortality. Front Public Health. 2020;8:152. [PubMed: 32411652]
67. deAlmeida AC, van Oort RJ and Wehrens XHT. Transverse aortic constriction in mice. Journal of visualized experiments : JoVE. 2010:1729. [PubMed: 20410870]
68. Park CS, Chen S, Lee H, Cha H, Oh JG, Hong S, Han P, Ginsburg KS, Jin S, Park I, Singh VP, Wang H-S, Franzini-Armstrong C, Park WJ, Bers DM, Kranias EG, Cho C and Kim DH. Targeted ablation of the histidine-rich Ca(2+)-binding protein (HRC) gene is associated with abnormal SR Ca(2+)-cycling and severe pathology under pressure-overload stress. Basic research in cardiology. 2013;108:344–344. [PubMed: 23553082]

Author Manuscript Author Manuscript Author Manuscript Author Manuscript

69. Skrbic B, Engebretsen KVT, Strand ME, Lunde IG, Herum KM, Marstein HS, Sjaastad I, Lunde PK, Carlson CR, Christensen G, Bjørnstad JL and Tønnessen T. Lack of collagen VIII reduces fibrosis and promotes early mortality and cardiac dilatation in pressure overload in mice†. Cardiovascular research. 2015;106:32–42. [PubMed: 25694587]

70. Xia Y, Dobaczewski M, Gonzalez-Quesada C, Chen W, Biernacka A, Li N, Lee DW and Frangogiannis NG. Endogenous thrombospondin 1 protects the pressure-overloaded myocardium by modulating fibroblast phenotype and matrix metabolism. Hypertension. 2011;58:902–11. [PubMed: 21947471]

71. Meguro T, Hong C, Asai K, Takagi G, McKinsey TA, Olson EN and Vatner SF. Cyclosporine attenuates pressure-overload hypertrophy in mice while enhancing susceptibility to decompensation and heart failure. Circulation research. 1999;84:735–40. [PubMed: 10189362]

72. Hölschermann H, Kohl O, Maus U, Dürfeld F, Bierhaus A, Nawroth PP, Lohmeyer J, Tillmanns H and Haberbosch W. Cyclosporin A Inhibits Monocyte Tissue Factor Activation in Cardiac Transplant Recipients. 1997;96:4232–4238.

73. Chen T, Guo J, Yang M, Han C, Zhang M, Chen W, Liu Q, Wang J and Cao X. Cyclosporin A impairs dendritic cell migration by regulating chemokine receptor expression and inhibiting cyclooxygenase-2 expression. Blood. 2004;103:413–21. [PubMed: 14504089]

74. Spisani S, Fabbri E, Muccinelli M, Cariani A, Barbin L, Trotta F and Dovigo L. Inhibition of neutrophil responses by cyclosporin A. An insight into molecular mechanisms. Rheumatology (Oxford). 2001;40:794–800. [PubMed: 11477284]

75. Tang J, Frey JM, Wilson CL, Moncada-Pazos A, Levet C, Freeman M, Rosenfeld ME, Stanley ER, Raines EW and Bornfeldt KE. Neutrophil and Macrophage Cell Surface Colony-Stimulating Factor 1 Shed by ADAM17 Drives Mouse Macrophage Proliferation in Acute and Chronic Inflammation. Molecular and cellular biology. 2018;38.

76. Yang W, Tao Y, Wu Y, Zhao X, Ye W, Zhao D, Fu L, Tian C, Yang J, He F and Tang L. Neutrophils promote the development of reparative macrophages mediated by ROS to orchestrate liver repair. Nat Commun. 2019; 10:1076. [PubMed: 30842418]

77. Gomez I, Duval V and Silvestre JS. Cardiomyocytes and Macrophages Discourse on the Method to Govern Cardiac Repair. Front Cardiovasc Med. 2018;5:134. [PubMed: 30333983]

78. Chen Y, Guo H, Xu D, Xu X, Wang H, Hu X, Lu Z, Kwak D, Xu Y, Gunther R, Huo Y and Weir EK. Left ventricular failure produces profound lung remodeling and pulmonary hypertension in mice: heart failure causes severe lung disease. Hypertension. 2012;59:1170–8. [PubMed: 22508832]

79. Guazzi M Pulmonary hypertension in heart failure preserved ejection fraction: prevalence, pathophysiology, and clinical perspectives. Circulation Heart failure. 2014;7:367–77. [PubMed: 24643889]

80. Thompson RB, Pagano JJ, Chow K, Sekowski V, Paterson I, Ezekowitz J, Anderson T, Dyck JRB and Haykowsky MJ. Subclinical Pulmonary Edema Is Associated With Reduced Exercise Capacity in HFpEF and HFrEF. Journal of the American College of Cardiology. 2017;70:1827. [PubMed: 28958338]

81. Guazzi M, Gomberg-Maitland M and Arena R. Pulmonary hypertension in heart failure with preserved ejection fraction. The Journal of heart and lung transplantation : the official publication of the International Society for Heart Transplantation. 2015;34:273–81.

82. Royce-Nagel G and Karamchandani K. Pulmonary Edema and Diastolic Heart Failure in the Perioperative Period. Case Rep Anesthesiol. 2018;2018:5101534. [PubMed: 29607222]

83. Russo C, Jin Z, Homma S, Rundek T, Elkind MS, Sacco RL and Di Tullio MR. Effect of obesity and overweight on left ventricular diastolic function: a community-based study in an elderly cohort. Journal of the American College of Cardiology. 2011;57:1368–74. [PubMed: 21414533]

84. Kishi S, Armstrong A, Venkatesh BA, Gidding S, Carr J, Jacobs D, Liu K, Goff D and Lima J. ASSOCIATION OF OBESITY WITH DIASTOLIC DYSFUNCTION IN EARLY ADULTHOOD: THE CARDIA STUDY. Journal of the American College of Cardiology. 2013;61:E864.

85. Alex L, Russo I, Holoborodko V and Frangogiannis NG. Characterization of a mouse model of obesity-related fibrotic cardiomyopathy that recapitulates features of human heart failure with

Author Manuscript Author Manuscript Author Manuscript Author Manuscript

preserved ejection fraction. American Journal of Physiology-Heart and Circulatory Physiology. 2018;315:H934–H949. [PubMed: 30004258]

86. Huynh K, McMullen JR, Julius TL, Tan JW, Love JE, Cemerlang N, Kiriazis H, Du XJ and Ritchie RH. Cardiac-specific IGF-1 receptor transgenic expression protects against cardiac fibrosis and diastolic dysfunction in a mouse model of diabetic cardiomyopathy. Diabetes. 2010;59:1512–20. [PubMed: 20215428]
87. Li Q, Wu S, Li SY, Lopez FL, Du M, Kajstura J, Anversa P and Ren J. Cardiac-specific overexpression of insulin-like growth factor 1 attenuates aging-associated cardiac diastolic contractile dysfunction and protein damage. American journal of physiology Heart and circulatory physiology. 2007;292:H1398–403. [PubMed: 17085535]
88. Hulsmans M, Clauss S, Xiao L, Aguirre AD, King KR, Hanley A, Hucker WJ, Wulfers EM, Seemann G, Courties G, Iwamoto Y, Sun Y, Savol AJ, Sager HB, Lavine KJ, Fishbein GA, Capen DE, Da Silva N, Miquerol L, Wakimoto H, Seidman CE, Seidman JG, Sadreyev RI, Naxerova K, Mitchell RN, Brown D, Libby P, Weissleder R, Swirski FK, Kohl P, Vinegoni C, Milan DJ, Ellinor PT and Nahrendorf M. Macrophages Facilitate Electrical Conduction in the Heart. Cell. 2017;169:510–522 e20. [PubMed: 28431249]
89. Xia Y, Lee K, Li N, Corbett D, Mendoza L and Frangogiannis NG. Characterization of the inflammatory and fibrotic response in a mouse model of cardiac pressure overload. Histochemistry and cell biology. 2009;131:471–81. [PubMed: 19030868]
90. Ryzhov S, Zhang Q, Biaggioni I and Feoktistov I. Adenosine A2B receptors on cardiac stem cell antigen (Sca)-1-positive stromal cells play a protective role in myocardial infarction. The American journal of pathology. 2013;183:665–72. [PubMed: 23827818]
91. Oka T, Akazawa H, Naito AT and Komuro I. Angiogenesis and cardiac hypertrophy: maintenance of cardiac function and causative roles in heart failure. Circulation research. 2014; 114:565–71. [PubMed: 24481846]
92. Walsh K and Shiojima I. Cardiac growth and angiogenesis coordinated by intertissue interactions. The Journal of clinical investigation. 2007;117:3176–9. [PubMed: 17975662]
93. Kivelä R, Hemanthakumar Karthik A, Vaparanta K, Robciuc M, Izumiya Y, Kidoya H, Takakura N, Peng X, Sawyer Douglas B, Elenius K, Walsh K and Alitalo K. Endothelial Cells Regulate Physiological Cardiomyocyte Growth via VEGFR2-Mediated Paracrine Signaling. Circulation. 2019;139:2570–2584. [PubMed: 30922063]
94. Zeriouh M, Sabashnikov A, Tenbrock A, Neef K, Merkle J, Eghbalzadeh K, Weber C, Liakopoulos OJ, Deppe AC, Stamm C, Cowan DB, Wahlers T and Choi YH. Dysregulation of proangiogeneic factors in pressure-overload left-ventricular hypertrophy results in inadequate capillary growth. Ther Adv Cardiovasc Dis. 2019;13:1753944719841795.
95. Shigematsu S, Yamauchi K, Nakajima K, Iijima S, Aizawa T and Hashizume K. IGF-1 regulates migration and angiogenesis of human endothelial cells. Endocr J. 1999;46 Suppl:S59–62. [PubMed: 12054122]
96. La Bach. Endothelial cells and the IGF system. J Mol Endocrinol. 2015;54:R1–13. [PubMed: 25351818]
97. Tonkin J, Temmerman L, Sampson RD, Gallego-Colon E, Barberi L, Bilbao D, Schneider MD, Musaro A and Rosenthal N. Monocyte/Macrophage-derived IGF-1 Orchestrates Murine Skeletal Muscle Regeneration and Modulates Autocrine Polarization. Mol Ther. 2015;23:1189–1200. [PubMed: 25896247]
98. Wang X, Zhao W, Ransohoff RM and Zhou L. Infiltrating macrophages are broadly activated at the early stage to support acute skeletal muscle injury repair. Journal of neuroimmunology. 2018;317:55–66. [PubMed: 29325905]
99. Arnold L, Henry A, Poron F, Baba-Amer Y, van Rooijen N, Plonquet A, Gherardi RK and Chazaud B. Inflammatory monocytes recruited after skeletal muscle injury switch into antiinflammatory macrophages to support myogenesis. The Journal of experimental medicine. 2007;204:1057–1069. [PubMed: 17485518]
100. Lu H, Huang D, Ransohoff RM and Zhou L. Acute skeletal muscle injury: CCL2 expression by both monocytes and injured muscle is required for repair. FASEb journal : official publication of the Federation of American Societies for Experimental Biology. 2011;25:3344–3355. [PubMed: 21697550]

Author Manuscript Author Manuscript Author Manuscript Author Manuscript

101. Takeda N, Manabe I, Uchino Y, Eguchi K, Matsumoto S, Nishimura S, Shindo T, Sano M, Otsu K, Snider P, Conway SJ and Nagai R. Cardiac fibroblasts are essential for the adaptive response of the murine heart to pressure overload. The Journal of clinical investigation. 2010; 120:254–65. [PubMed: 20038803]

102. Vinciguerra M, Santini MP, Claycomb WC, Ladurner AG and Rosenthal N. Local IGF-1 isoform protects cardiomyocytes from hypertrophic and oxidative stresses via SirT1 activity. Aging (Albany nY). 2009;2:43–62. [PubMed: 20228935]

103. Samarel AM. IGF-1 Overexpression rescues the failing heart. Circulation research. 2002;90:631–3. [PubMed: 11934828]

Author Manuscript Author Manuscript Author Manuscript Author Manuscript

HIGHLIGHTS

- ErbB3 receptors are expressed on myeloid cells in blood, spleen, and heart. The level of ErbB3 cell surface expression is higher on cardiac myeloid cells compared to cells in blood and spleen.
- Transverse aortic constriction induced rapid, within three days after surgery, accumulation of myeloid cells in the heart.
- Genetic ablation of myeloid cell-specific ErbB3 signaling resulted in the development of acute heart failure in male but not female mice.
- At the cellular level, male mice with ErbB3 deletion were characterized by the reduced intramyocardial accumulation of neutrophils and monocytes, decreased proliferation of Sca-1 positive cells, and production of IGF-1.
- NRG-1, an ErbB receptor ligand, induced migration in myeloid cells from control animals but not from mice with ErbB3 deletion.

Author Manuscript Author Manuscript Author Manuscript Author Manuscript

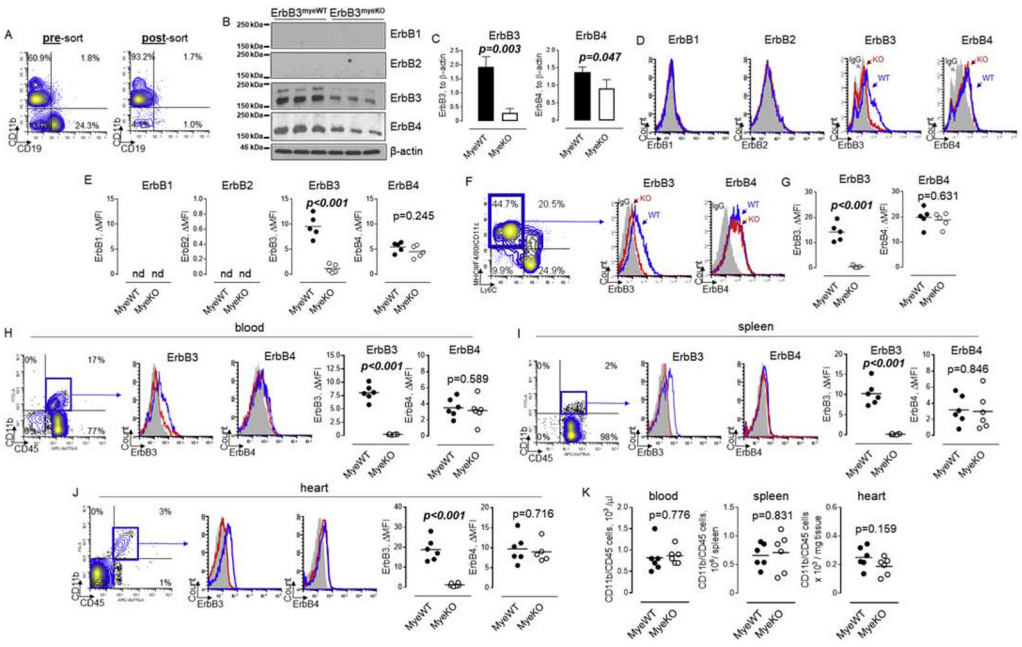

Figure 1. Number of myeloid cells are similar between ErbB3^{MyeWT} and ErbB3^{MyeKO} mice in steady-state conditions.

A. Bone marrow cells were isolated from femur and tibia bones (left and right legs) and used to isolate CD11b positive cells as described in Methods. Representative flow cytometry contour plots showing enrichment of CD11b cells after immunomagnetic separation. **B**. Western blot analysis of ErbB receptors protein expression in bone marrow CD11b cells obtained from wild type and ErbB3 knockout animals. The horizontal lines on the left are the molecular weight ladder. **C**. Graphical representation of data from western blot analysis of ErbB receptors expression in wild type (*MyeWT, n=3*) and myeloid cell-specific ErbB3 knockout (*MyeKO, n=3*) mice. Data are shown as mean±SEM, statistical significance calculated using unpaired *t* test. **D**. Representative flow cytometry histograms demonstrating cell surface expression of ErbB receptors in bone marrow CD11b cells. *Shaded histograms* – IgG control; *open blue histograms – wild type mice; open red histograms – knockout animals*. **E**. Graphical representation of flow cytometry data on ErbB receptors expression in bone marrow CD11b cells obtained from wild type (*MyeWT, n=5*) or ErbB3 knockout (*MyeKO, n=5*) mice, unpaired *t* test. **F**. Bone marrow Lin- hematopoietic progenitor cells were incubated in the presence of 20 ng/ml of GM-CSF for six days to generate proinflammatory macrophages (*left contour plot, blue gate*). Levels of ErbB3 (*middle histogram*) and ErbB4 (*right histogram*) were determined using flow cytometry. **G**. Data from flow cytometric analysis of cell surface expression of ErbB3 and ErbB4 on BM-derived macrophages generated in the presence of GM-CSF. **H- J**. Representative flow cytometry plots showing the percentage of CD11b^{pos}CD45^{pos} myeloid cells (*contour plots, left*), expression of ErbB3 receptors (*histograms, left*), and ErbB4 (*histograms, right*) on myeloid cells in peripheral blood (**H**), spleen (**I**), and heart (**J**) of wild type (*MyeWT, blue histograms*) and ErbB3 knockout (*MyeKO, red histograms*) animals. *Shaded histograms* – IgG control. **K**. Data from flow cytometric analysis showing the number of myeloid cells in

Author Manuscript Author Manuscript Author Manuscript Author Manuscript

blood, spleen, and heart isolated from control mice (MyeWT, *n=6*) and myeloid cells-specific ErbB3 knockout (*MyeKO, n=6*) animals. Unpaired *t* test.

Author Manuscript Author Manuscript Author Manuscript Author Manuscript

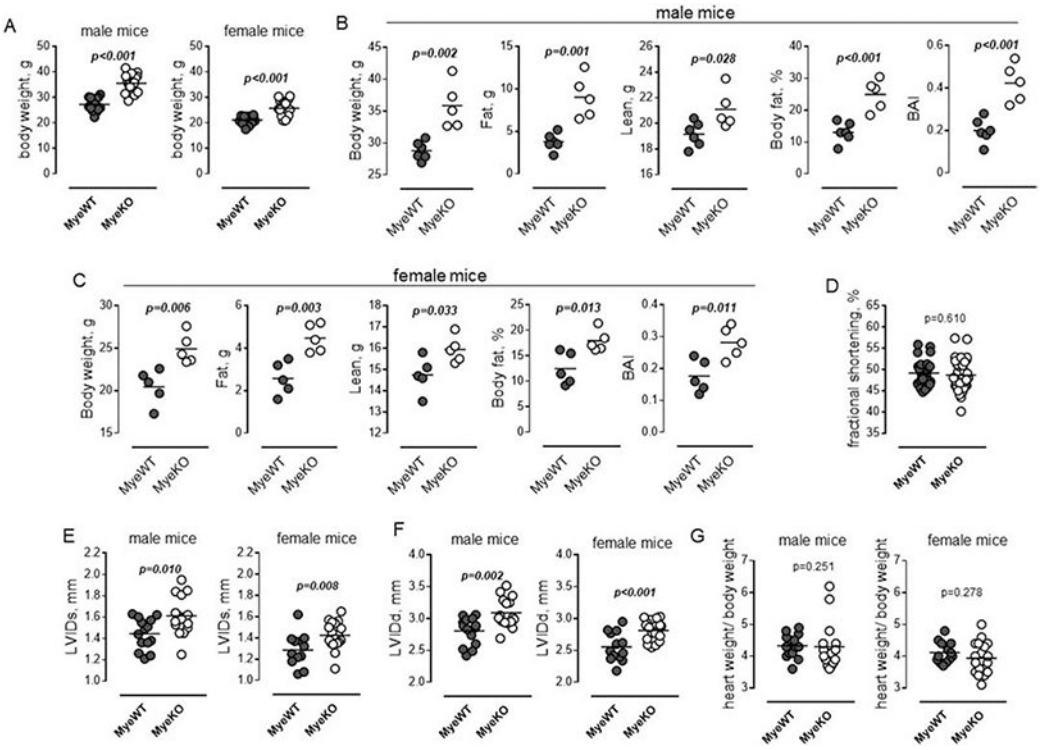

Figure 2. ErbB3^{MyeKO} mice show higher weight but no differences in cardiac function at baseline.

A. Body weight of 15-week old male (*left*) ErbB3^{MyeWT} (*n=14*) and ErbB3^{MyeKO} (*n=16*) and female (*right*) ErbB3^{MyeWT} (*n=13*) and ErbB3^{MyeKO} (*n=18*) mice. Unpaired *t* test. **B-C**. Fat and lean tissue composition in male (**B**) and female (**C**) mice were determined using NMR as described in Methods. Body fat percentage was calculated by dividing fat mass by body weight; BAI (body adiposity index) as a ratio of fat mass to lean mass; n=5, unpaired *t* test. **D**. Fractional shortening in MyeWT (*n=27*) and MyeKO (*n=34*) animals (*males and females*). Unpaired *t* test. **E-G**. Left ventricular end-systolic (**E**) and end-diastolic diameters (**F**) in male (*left*) and female (*right*) mice. **G**. Heart-to-body weight ratios in male (*left*) and female (*right*) mice. **E-G**. *n=14*, male ErbB3^{MyeWT}; *n=16*, male ErbB3^{MyeKO}; *n=13*, female ErbB3^{MyeWT}; *n=18*, female ErbB3^{MyeKO} mice; **D-H**. Horizontal lines are indicating mean values. Statistical significance was calculated using unpaired *t* test.

Author Manuscript Author Manuscript Author Manuscript Author Manuscript

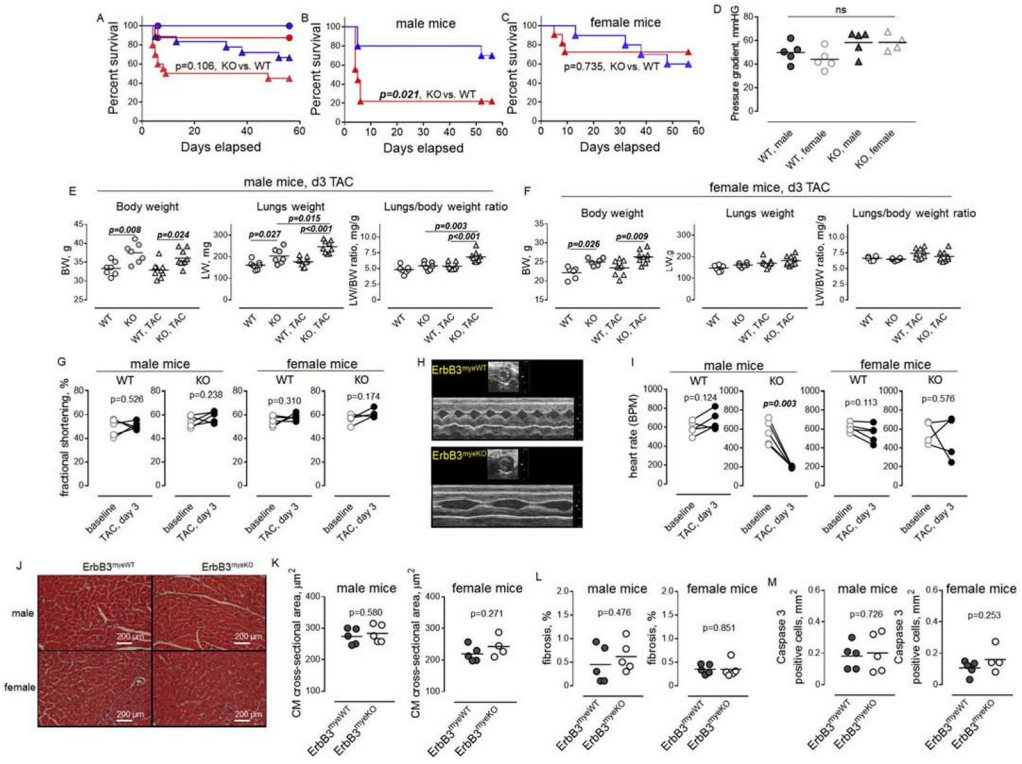

Figure 3. Transverse aortic constriction leads to increased early mortality in ErbB3^{MyeKO} males but not in control or ErbB3^{MyeKO} female mice.

A-C. Log-rank (Mantel-Cox) analysis of survival rate for (**A**) sham-operated control type (*n= 8, blue line and circles*) and ErbB3^{MyeKO} (*n=12, red line and circles*) and TAC (*n= 18, control, blue triangles; n= 20, MyeKO, red triangles*) groups of male and female mice, (**B**) male ErbB3^{myeWT} (*n=9, blue*) and ErbB3^{MyeKO} (*n=9, red*), and (**C**) female ErbB3^{myeWT} (*n=9, blue*) and ErbB3^{MyeKO} (*n=11, red*) mice. *P* values are indicated. **D**. Doppler measurements of pressure gradient at day 3 after TAC. **E-F**. Body weight (left), lungs weight (middle) and lungs-to-body weight ratios (right) in ErbB3^{myeWT} (*open*) and ErbB3^{MyeKO} (*grey-shaded*) male (**E**) and female (**F**) mice. *Circles*-sham-operated animals; *Triangles* - day 3 after TAC surgery. Sham - *n=7*, male ErbB3^{MyeWT}; *n=7*, male ErbB3^{MyeKO}; *n=6*, female ErbB3^{MyeWT}; *n=6*, female ErbB3^{MyeKO} mice; day 3 post TAC - *n=9*, male ErbB3^{MyeWT}; *n=9*, male ErbB3^{MyeKO}; *n=9*, female ErbB3^{MyeWT}; *n=9,* female ErbB3^{MyeKO} mice. Horizontal lines indicate mean values. One-way ANOVA, Tukey's multiple comparisons test. **G**. Fractional shortening before (*baseline*) and on day 3 post-TAC in wild type male (*n=5*) and female (*n=6*) mice, and ErbB3 knockout male (*n=5*) and female (*n=4*) animals. Paired *t* test. **H**. Representative echocardiograms recorded on day 3 post-TAC in wild-type (*upper panel*) and ErbB3 knockout (*lower panel*) male mice. **I**. Graphical representation of heart rate, paired *t* test. **J**. Representative H&E staining of heart sections 3 days after TAC. **K-M**. Graphical representation of cross-sectional area of H&E stained cardiomyocytes (**K**), myocardial fibrosis after Masson's Trichrome staining (**L**), and immunohistochemical staining of caspase 3 (**M**). Unpaired *t* test.

Author Manuscript Author Manuscript Author Manuscript Author Manuscript

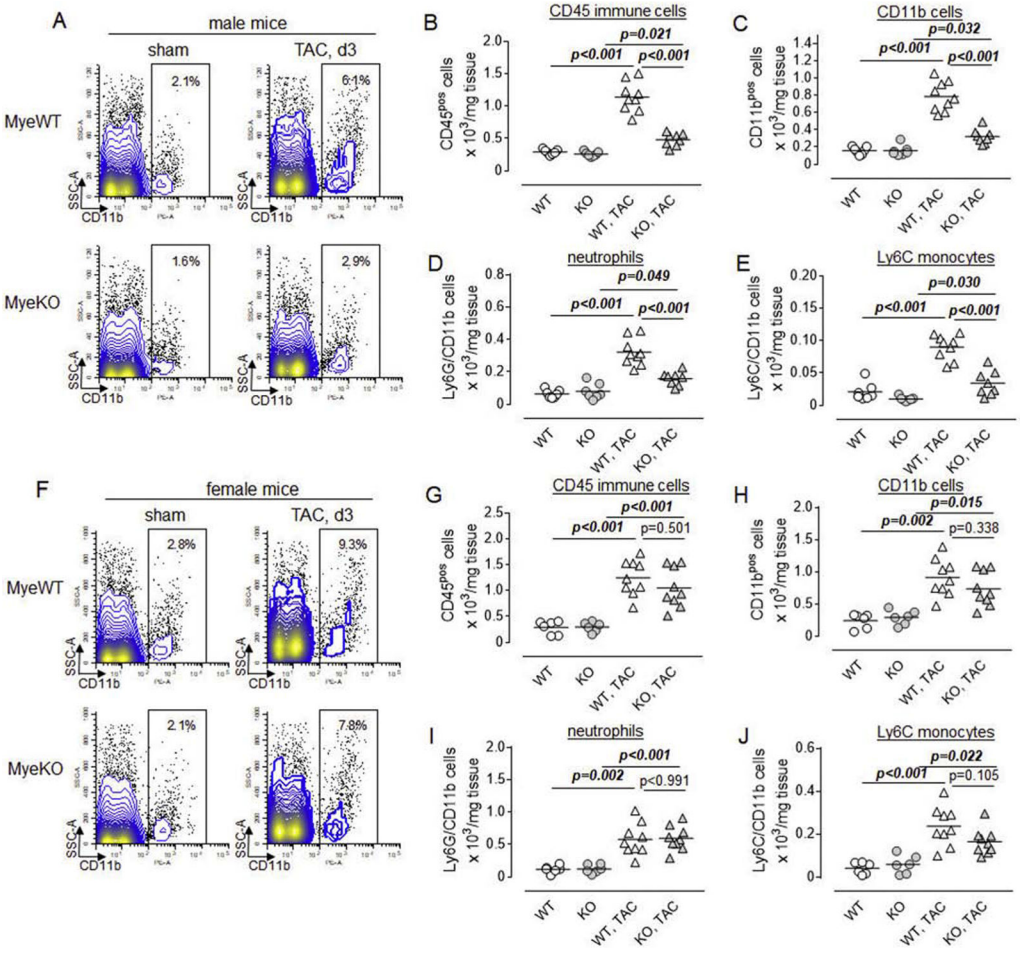

Figure 4. Transverse aortic constriction is associated with the accumulation of myeloid cells in the hearts of control but not in ErbB3^{MyeKO} male mice.

A. Representative flow cytometry contour and dot plots showing the percentage of CD11b positive myeloid cells (*black rectangle gate*) in control (MyeWT, *upper panel*) and ErbB3 knockout (MyeKO, *lower panel*) male mice. **B-E**. Graphical representation of flow cytometric data showing the total number of (**B**) CD45 immune cells, (**C**) CD11b myeloid cells, (**D**) Ly6G^{pos}CD11b^{pos} neutrophils, and (**E**) Ly6C^{pos}CD11b^{pos}Ly6G^{neg} monocytes in control (WT, *open*) and myeloid cell-specific ErbB3 knockout (KO, *grey-shaded*) male mice before (*n=7*, control; *n=7*, KO) and on day 3 post-TAC (*n=9*, control; *n=8*, KO). **F-J**. Flow cytometry plots (**F**) and the total number of (**G**) immune cells, (**H**) myeloid cells, (**I**), neutrophils, and (**J**) proinflammatory monocytes in female mice; Sham - *n=6*, control; *n=6*, KO; day 3 post-TAC - *n=9*, control; *n=9*, KO. Horizontal lines-mean values. One-way ANOVA, Tukey's multiple comparisons test.

Author Manuscript Author Manuscript Author Manuscript Author Manuscript

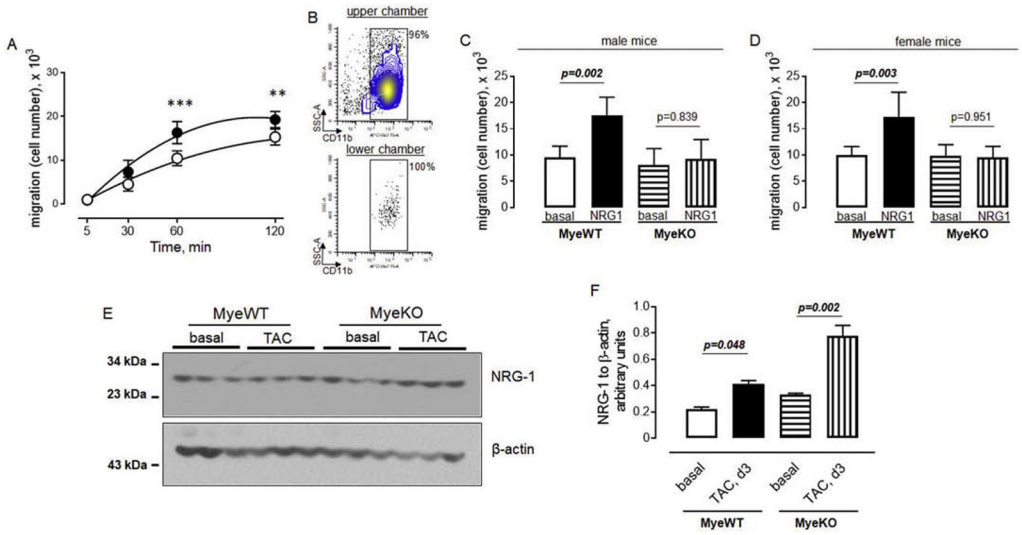

Figure 5. Neuregulin-1/ErbB3 signaling promotes the migration of myeloid cells.

Bone marrow CD11b positive myeloid cells were purified as described in the Methods section. **A**. The number of cells in the lower chamber of the transwell system in the absence (*open circles*) or presence (*closed circles*) of 50 ng/ml of recombinant NRG-1. *n=5*, ***p<0.01*; ****p<0.001*, One-way ANOVA, Tukey's multiple comparisons test. **B**. Flow cytometric plots showing the percent of myeloid cells in upper and lower chambers of the transwell system after 60 min of incubation in the presence of 50 ng/ml of recombinant NRG-1. **C-D**. The effect of 50 ng/ml of recombinant NRG-1 on the migration of myeloid cells obtained from ErbB3^{MyeWT} and ErbB3^{MyeKO} male (**C**) and female (**D**) mice. *n=6*, One-way ANOVA, Tukey's multiple comparisons test. **E-F**. Western blot analysis (**E**) and graphical representation (**F**) of NRG-1 protein levels in hearts isolated from wild type (*MyeWT*) or ErbB3 knockout (*MyeKO*) males before and on day 3 post-TAC; Data are shown as mean±SEM, n=3, One-way ANOVA, Tukey's multiple comparisons test.

Author Manuscript Author Manuscript Author Manuscript Author Manuscript

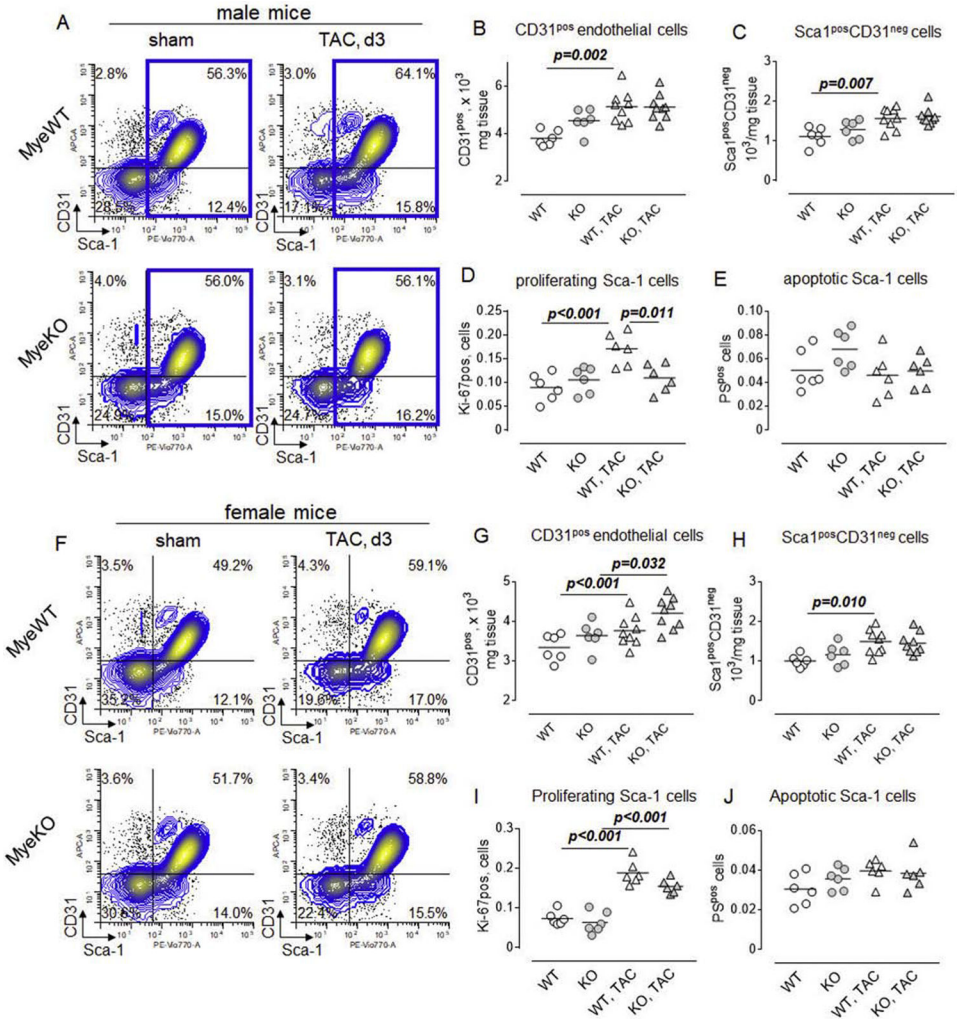

Figure 6. Increased proliferation of cardiac Sca-1 non-immune cells in control but not in ErbB3^{MyeKO} male mice.

A. Representative flow cytometry plots demonstrating the percentage of CD31^{pos}Sca-1^{pos} endothelial cells (*upper right quadrant*) and Sca1^{pos}CD31^{neg} cardiac fibroblasts (*lower right*), within CD45 negative (non-immune population) in control (MyeWT, *upper panel*) and ErbB3 knockout (MyeKO, *lower panel*) male mice. The population of Sca-1 positive non-immune cells is shown in the blue gate. **B-E**. Total number of (**B**) endothelial cells, (**C**) Sca-1 ^{pos}CD31^{neg} cells, (**D**) proliferating Sca-1 positive cells (blue gate), and (**E**) apoptotic Sca-1 positive cells, defined as a phosphatidylserine (PS) positive cells, within the blue gate in control (WT, *open*) and myeloid cell-specific ErbB3 knockout (KO, *grey-shaded*) male mice. Sham - *n=7*, control; *n=7*, KO; day 3 after TAC - *n=9*, control; *n=8*, KO. F-J. Flow cytometry plots (**F**) and the total number of (**G**) endothelial cells, (**H**) cardiac fibroblasts, (**I**) proliferating and (**J**) apoptotic Sca-1 positive cells in female mice. Sham - *n=6*, control; *n=6*, KO, and on day 3 post-TAC - *n=9*, control; *n=9*, KO. Horizontal lines are mean values. One-way ANOVA, Tukey's multiple comparisons test.

Author Manuscript Author Manuscript Author Manuscript Author Manuscript

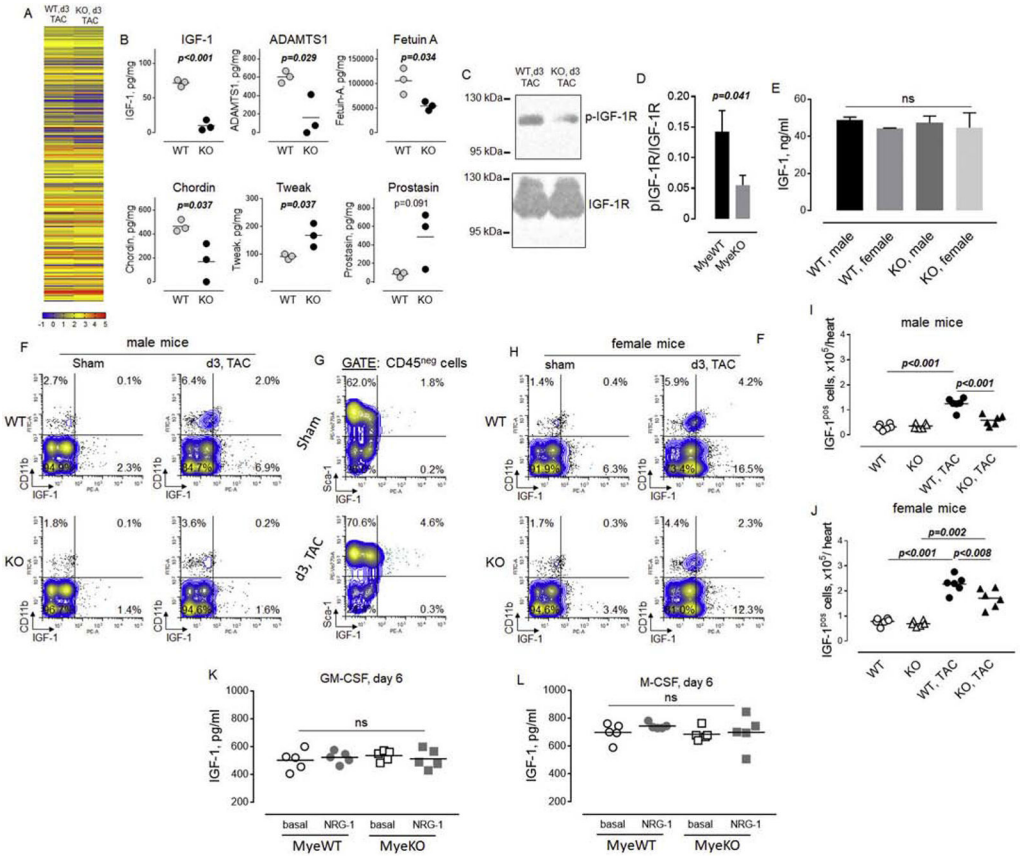

Figure 7. A higher number of IGF-1 producing cells in hearts from control but not in ErbB3^{MyeKO} male mice after TAC.

Hearts from control and ErbB3^{MyeKO} mice were isolated from animals at day 3 after TAC and homogenized in RIPA buffer. Lysates were cleared using centrifugation and used to perform quantitative antibody array analysis as described in Methods. **A**. Heatmap of the relative levels of protein expression in hearts of ErbB3^{MyeWT} (WT, *n=3*) and ErbB3 knockout (KO, *n=3*) male mice on day 3 after TAC. Heatmap color key with six different colors ranging from one-tenth of pictogram (blue) to hundreds of a nanogram (red) of proteins level. The numbers associated with a color key are showing arguments of the decimal logarithm of protein concentrations. **B**. Proteins that demonstrated significant differences between control (WT) and myeloid cell-specific ErbB3 knockout (KO) mice in quantitative antibody array. Unpaired *t* test. **C**. Western blot analysis of phosphorylated IGF-1R (*p-IGF-1R, upper panel*) and total IGF-1R (*lower panel*) protein expression in hearts isolated from wild type and ErbB3 knockout animals on day 3 post-TAC. The horizontal lines on the left are the molecular weight ladder. **D**. Graphical representation of data from western blot analysis; arbitrary units; MyeWT, *n=6*, MyeKO, *n=6*. Data are shown as mean ±SEM; statistical significance calculated using unpaired *t* test. **E**. Levels of IGF-1 in peripheral blood of male and female animals on day 3 post-TAC.One-way ANOVA; *ns* - not significant. **F**. Representative flow cytometric plots showing the percentage of IGF-1 producing cells in cell suspensions obtained from control (WT, *upper panel*) and ErbB3^{MyeKO}(KO, *lower panel*) male mice. **G**. Flow cytometric plots showing the percentage of IGF-1 producing cells in subpopulation of Sca-1 positive cells in sham-operated mice and

Author Manuscript Author Manuscript Author Manuscript Author Manuscript

TAC control animals. **H**. Flow cytometric plots showing the percentage of IGF-1 producing cells in cell suspensions obtained from control (WT, *upper panel*) and ErbB3^{MyeKO} (KO, *lower panel*) female mice. **I-J**. Data from flow cytometric analysis of IGF-1 producing cells in male (**I**, *n=6 per group*) and female (**J**, *n=6 per group*). One-way ANOVA, Tukey's multiple comparisons test. **K-L**. IGF-1 levels measured in the supernatant of Lin- bone marrow cells isolated from wild type (*MyeWT*) or ErbB3 knockout (*MyeKO*) mice after incubation with 20 ng/ml of GM-CSF (**K**) or M-CSF (**L**) for 6 days. One-way ANOVA; *ns* - not significant.